Global and Planetary Change 261 (2026) 105414

Contents lists available at ScienceDirect

Global and Planetary Change

journal homepage: www.elsevier.com/locate/gloplacha

Research Article

Long-term variations in palaeoenvironmental conditions in the Western Tethys during the late Aptian–late Cenomanian time interval: From an unstable to a stable ocean

Gabriele Gambacorta[a,*], Philipp Böning[b], Cinzia Bottini[c], Hans-Jürgen Brumsack[b], Elisabetta Erba[c]

[a] Dipartimento di Scienze della Terra, Università degli Studi di Firenze, Via G. La Pira 4, 50121 Florence, Italy
[b] Institute for Chemistry and Biology of the Marine Environment (ICBM), University of Oldenburg, Ammerländer Heerstrasse 114-118, 26129 Oldenburg, Germany
[c] Dipartimento di Scienze della Terra, Università degli Studi di Milano, Via Mangiagalli 34, 20133 Milan, Italy

ARTICLE INFO

Editor: DR Haijun Song

Keywords:
Cretaceous
Pelagic sedimentation
Inorganic geochemistry
Umbria-Marche Basin
Western Tethys

ABSTRACT

A high-resolution record of long-term variations in detrital input, chemical weathering, freshwater influx, and palaeoproductivity from a pelagic environment of the Western Tethys spanning the late Aptian to late Cenomanian (~25 million years) is presented, based on quantitative elemental data from the Umbria-Marche Basin (Monte Petrano section and Piobbico Core, central Italy). This interval captures a major environmental transition from the multicolored marlstone and black shale-dominated sediments of the Marne a Fucoidi Formation to the extensive limy deposits of the Scaglia Bianca Formation but also highlights three main distinct palaeoenvironmental phases during the deposition of the Marne a Fucoidi. During the late Aptian cooling episode, semi-arid conditions prevailed, with surface waters being oligo- to mesotrophic and stratified, while bottom waters remained oxygenated. A marked warming started at the Aptian/Albian boundary paralleled by increased surface water fertility and seafloor deoxygenation. The early to middle Albian experienced intensified weathering and nutrient supply under warm and humid conditions, fostering meso- to eutrophic conditions and promoting the deposition of alternated marlstones and black shales. A major transition took place in the late Albian, with the emergence of arid conditions that reduced runoff and chemical weathering, coinciding with progressively more oligotrophic surface waters and a stable thermocline that persisted until just prior to the onset of Oceanic Anoxic Event 2 in the latest Cenomanian.

1. Introduction

The mid-Cretaceous (~120–90 Ma) was characterized by a warm climate, minimal temperature differences across latitudes, and absence of permanent ice sheets (e.g., Clarke and Jenkyns, 1999; Föllmi, 2012; Friedrich et al., 2012; Bodin et al., 2015; O'Brien et al., 2017 and references therein; Bottini and Erba, 2018). Sea-surface temperatures (SSTs) at low latitudes are estimated to have ranged between 25° and 40 °C (O'Brien et al., 2017 and references therein), with prevailing warm conditions punctuated by cooling interludes (e.g., Kemper, 1987; Weissert and Lini, 1991; Hochuli et al., 1999; Price, 1999; Herrle and Mutterlose, 2003; Mutterlose et al., 2009; McAnena et al., 2013; Millán et al., 2014; Bottini et al., 2015; Bottini and Erba, 2018). The Aptian–Turonian interval (~121.4–89.4 Ma, Gradstein et al., 2020) was marked by major perturbations in the global carbon cycle, associated with transient but sometimes prolonged palaeoclimatic and palaeoceanographic disruptions, characterized by widespread seafloor anoxia. These events, known as Oceanic Anoxic Events (OAEs) (Schlanger and Jenkyns, 1976; see Jenkyns, 2010 for a review) include the early Aptian OAE 1a (e.g., Weissert, 1989; Menegatti et al., 1998; Tejada et al., 2009; Bottini et al., 2012; Bauer et al., 2021, 2024; Sequero et al., 2026), the early Albian OAE 1b (e.g., Arthur et al., 1990; Herrle et al., 2004; Sabatino et al., 2015; Bodin et al., 2023), the latest Albian OAE 1d (e.g., Wilson and Norris, 2001; Robinson et al., 2008; Bornemann et al., 2017; Gambacorta et al., 2020; Li et al., 2026), and the Cenomanian/Turonian boundary interval OAE 2 (e.g., Scholle and Arthur, 1980; Jarvis et al., 2006, 2011; Jenkyns et al., 2017; Cui et al., 2025; Gambacorta et al., 2026; Liang et al., 2026; Zhang et al., 2026).

* Corresponding author.
E-mail address: gabriele.gambacorta@unifi.it (G. Gambacorta).

https://doi.org/10.1016/j.gloplacha.2026.105414
Received 16 November 2025; Received in revised form 26 February 2026; Accepted 5 March 2026
Available online 12 March 2026

Most studies covering the Aptian–Turonian interval have focused specifically on OAEs (e.g., Hetzel et al., 2009; Sabatino et al., 2015; Castro et al., 2019; Gambacorta et al., 2020; Blok et al., 2022; Guo et al., 2024) and short-lived events such as the mid-Cenomanian Event I (MCE I, e.g., Coccioni and Galeotti, 2003). In contrast, only a limited number of works have investigated long-term palaeoceanographic and palaeoclimatic trends across the late Aptian–Cenomanian interval. Among these, Giorgioni et al. (2012) investigated long-term palaeoceanographic variability, demonstrating through spectral analyses a dominant ~400 kyr cyclicity in the $\delta^{13}C$ record, consistent with Milankovitch long eccentricity forcing. Giorgioni et al. (2015) documented lithostratigraphic changes associated with the onset of mid-Cretaceous chalk/limy sedimentation; however, their interpretations were based exclusively on lithostratigraphic observations, without integrating geochemical or palaeontological proxies. Bottini and Erba (2018) reconstructed temperature and fertility variations across the uppermost Barremian–Cenomanian interval using calcareous nannofossil assemblages from the Umbria–Marche and Lombardy basins, thus primarily documenting surface-water variability.

Building upon these previous studies, here we present new elemental geochemical data from two pelagic successions—the Monte Petrano section and the Piobbico Core—from the Umbria–Marche Basin (Central Apennines, Italy). This multi-proxy dataset provides an integrated perspective on long-term variations in detrital input, continental runoff, climate, and palaeoproductivity in the Western Tethys. Our study aims to capture the long-term coupling between depositional processes and palaeoenvironmental changes during the late Aptian–late Cenomanian in the Western Tethys.

2. Geological setting and studied records

The Jurassic–Cretaceous pelagic sedimentary record of the Umbria-Marche Basin was deposited on the rifted continental margin of the Western Tethys (Channel et al., 1979) over a highly irregular sea floor (Bernoulli, 1972; Bernoulli and Jenkyns, 1974, 2009; Cresta et al., 1989; Alvarez, 1990) (Fig. 1). The Aptian to lowermost Turonian pelagic record is represented by the Marne a Fucoidi and Scaglia Bianca formations deposited in the northern tropical climatic belt (Dercourt et al., 2000; Skelton et al., 2003) at an estimated water depth of approximately 1500–2000 m (Arthur and Premoli Silva, 1982; Giraldo-Gómez et al., 2023).

The Marne a Fucoidi Fm. (Figs. 2A, B and 3), dated to the early Aptian–late Albian, is a rhythmic, varicolored pelagic succession consisting of marlstones, marly limestones, black shales, and minor proportions of limestones (Erba et al., 1989; Parisi et al., 1989). In particular, the upper Aptian interval is characterized by a rhythmic alternation of reddish and greenish marlstones and marly limestones (Fig. 2A). The middle–upper part of the Marne a Fucoidi Formation is characterized by a rhythmic alternation of black shales and yellowish-grey, and in some intervals red, marlstones and marly limestones (Herbert and Fischer, 1986; Premoli Silva et al., 1989; Erba, 1988, 1992; Galeotti et al., 2003; Tiraboschi et al., 2009) (Fig. 2B). Major black shales distinguish the lower Aptian Selli Level, which is the regional lithological expression of OAE 1a, the upper Aptian '113 Level', the Kilian Level at the Aptian/Albian boundary, and the lower Albian Urbino Level (OAE 1b) (e.g., Coccioni et al., 1987, 1989; Erba, 1988, 1992; Erba et al., 1989). Furthermore, an approximately 3-m-thick dark brown and argillaceous interval with black shales, called Monte Nerone Level, characterizes the lowermost Albian (Erba et al., 1989).

Directly above the Marne a Fucoidi Fm., the Scaglia Bianca Fm. (Figs. 2C and 3), of late Albian–early Turonian age, marks a shift in sedimentation to limestones and black shale-poor facies (Parisi et al., 1989), resulting from the lithification of nannofossil-planktonic foraminiferal oozes with intervals enriched in radiolarian tests (Gambacorta et al., 2015; Giorgioni et al., 2015). The lower lithostratigraphic boundary is located at the lowermost limestone with chert nodules (Parisi et al., 1989). The Scaglia Bianca Fm. contains sporadic black shales in particular in the upper Albian Pialli Level (Coccioni, 2001; Gambacorta et al., 2015, 2020), which correlates with the sedimentary expression of the lower part of OAE 1d, and from the mid-Cenomanian Event I (MCE I) (Coccioni and Galeotti, 2003; Gambacorta et al., 2015, 2016) up to the Bonarelli Level (Lanci et al., 2010), which is represented by approximately 1-m-thick interval of black shales and radiolarian-rich layers and is the regional sedimentary expression of the latest Cenomanian–earliest Turonian OAE 2.

The Monte Petrano section is located close to the Moria village (Schwarzacher, 1994; Giorgioni et al., 2012, 2015; Gambacorta et al., 2015, 2016). The studied interval covers the uppermost portion of the Marne a Fucoidi Fm. and the Scaglia Bianca Fm. up to the base of the Bonarelli Level (Giorgioni et al., 2012, 2015; Gambacorta et al., 2015). The section includes the upper part of the Marne a Fucoidi Formation, with a total thickness of ~28 m, characterized by variegated marlstones rhythmically alternating with black shales. This unit is overlain by the Scaglia Bianca Formation, which reaches a total thickness of about 70.5 m and is composed of whitish to locally pinkish pelagic limestones with chert nodules and bands, radiolarian layers, and sporadic black shales; ~65 m of this formation were analyzed here. The carbon isotope records allowed the identification of the positive $\delta^{13}C$ excursions associated with OAE 1d, the Mid-Cenomanian Event (MCE I), and OAE 2, as well as longer-term background variations (Giorgioni et al., 2012, 2015; Gambacorta et al., 2015). Calcareous nannofossil and planktonic foraminiferal biostratigraphy are documented in Gambacorta et al. (2015), Bottini and Erba (2018), and Petrizzo and Gilardoni (2020) and provide the biostratigraphic framework of the section by identifying nannofossil biozones CNC9b to CNC12 of Erba et al. (2026), which constrain the Albian–Cenomanian interval, and five planktonic foraminiferal

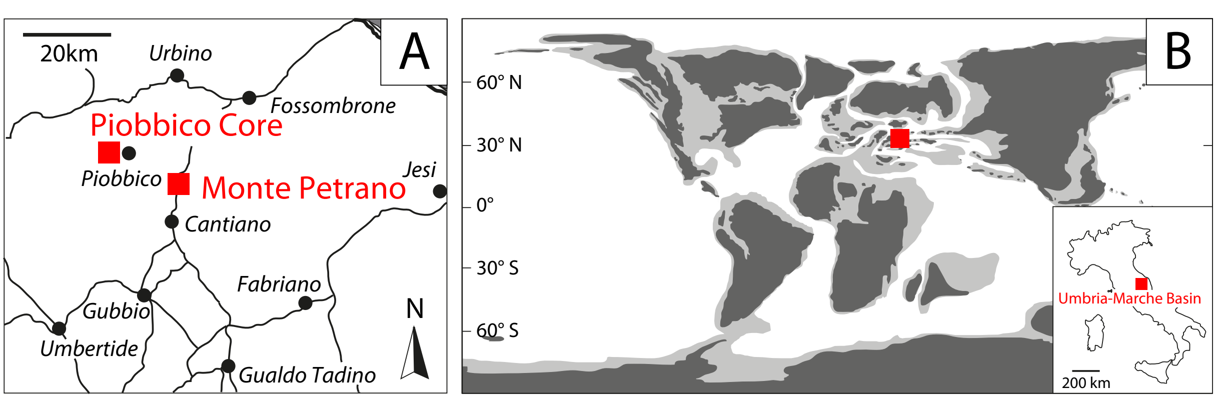

Fig. 1. A. Present-day location of studied records. B. Relative position of the Umbria-Marche Basin in the Cenomanian. Emerged lands in dark grey, shallow seas in light grey, deep seas in white (reconstruction based on R.C. Blakey, NAU Geology (https://deeptimemaps.com).

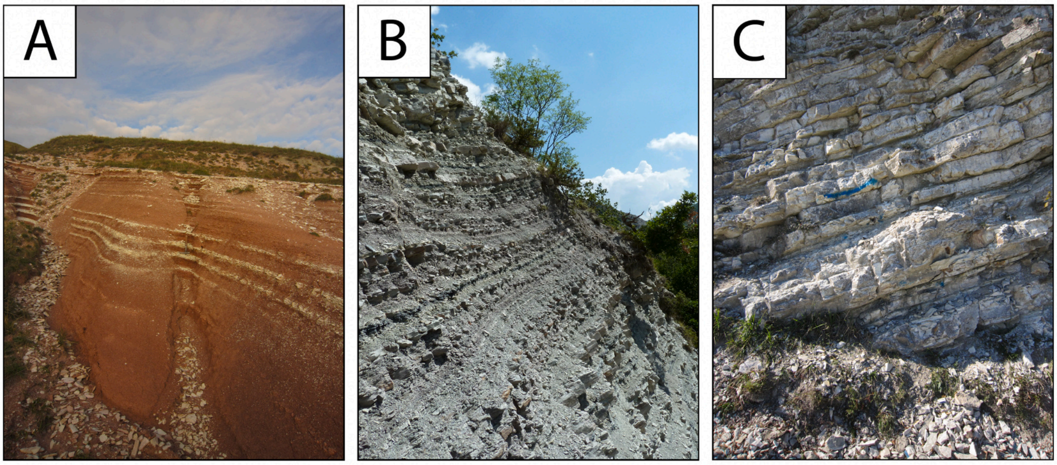

Fig. 2. Close-ups of the lithostratigraphic intervals investigated. A. Aptian interval of the Marne a Fucoidi Fm. characterized by rhythmic reddish-greenish marlstones/marly limestones (Monte Petrano). B. Cyclical black shale and marlstones/marly limestones of the lower–middle Albian interval of the Marne a Fucoidi Fm. (Le Brecce section, close to the coring site of the Piobbico Core). C. Limestone of the Scaglia Bianca Fm. (Monte Petrano).

biozones, ranging from *P. ticinensis* to *R. cushmani*, within the Scaglia Bianca Formation.

The Piobbico Core drill site is located at a locality called “Le Brecce”, 3 km west of the small town of Piobbico, at km 33 of Apecchiese State Road No. 257 (Erba, 1988). Continuous coring was performed through the lowermost part of the Scaglia Bianca, the entire Marne a Fucoidi Fm. and the uppermost part of the Maiolica Fm., with a 98.8% recovery. Calcareous nannofossil biostratigraphy documents four nannofossil biozones, from CNC6 to CNC9b of Erba et al. (2026), while planktonic foraminiferal biostratigraphy spans from the *G. duboisi/G. gottisi* Zone to the *P. buxtorfi* Zone (Erba, 1988, 1992; Tornaghi et al., 1989; Bottini et al., 2015; Bottini and Erba, 2018). C-stable isotope chemostratigraphy of the Piobbico Core documents high-resolution isotopic variability throughout the Aptian–Albian interval (Tiraboschi et al., 2009; Bottini et al., 2015; Erba et al., 2015; Giorgioni et al., 2015).

3. Material and methods

A composite record was obtained merging the upper Albian–uppermost Cenomanian succession of the Monte Petrano outcrop with the Aptian–upper Albian record of the Piobbico Core. We placed the 0 m level at the base of the Bonarelli Level. The studied interval of the Monte Petrano section covers the Scaglia Bianca Fm. from below the Bonarelli Level to the base of the formation, for a thickness of 65.2 m and the uppermost 8 m of the Marne a Fucoidi Fm. The Piobbico Core was studied from 9.27 m stratigraphic depth (corresponding to a stratigraphic position 8 m below the base of the Scaglia Bianca Fm. in the Monte Petrano section) down to the top of the carbon-isotopic segment ‘C7’ sensu Menegatti et al. (1998), equivalent to the top of isotopic segment ‘Ap7’ sensu Bottini et al. (2015). The two datasets were aligned at 9.27 m, which approximates the uppermost level of the Piobbico Core analyzed by Tiraboschi et al. (2009). A total of 285 samples, 155 samples from the Monte Petrano outcrop and 130 samples from the Piobbico Core, were collected approximately every 50 cm. To best capture the long-term variations within the studied record, we sampled limestones, marly limestones and marlstones, while avoiding marly claystone, radiolarian layers, chert nodules and bands, and black shales.

Samples were analyzed for elemental concentrations by X-ray fluorescence analysis (XRF) at the University of Oldenburg. About 700 mg of sample powder were mixed with 4200 mg lithium tetraborate, pre-oxidized in an oven at 500 °C overnight with NH_4NO_3 and then fused to glass beads. The beads were analyzed by a wave-length dispersive X-ray fluorescence (WD-XRF) spectrometer equipped with a rhodium tube (Axios Plus, Panalytical®). XRF measurements are based on a calibration with 48 certified and 7 in-house international reference samples covering a wide range in composition (Gäng et al., 2023). Analytical precision, checked using in-house standards, is better than 1% for Si, Ti, Al, Fe, Mg, Mn, Ca, K, P, Sr, 2% for Ba, Cr, Cu, Mo, Ni, Rb, V, Zn, Zr, and better than 5% for Na and Y, except As, Co, Pb (5–10%).

Elemental concentrations were normalized to Al to account for dilution effects. Concentrations are compared relative to the reference average crustal rocks or average shale (AS) element abundance of Wedepohl (1971, 1991) and expressed as element enrichment ($element_{EF}$).

Enrichment factors were computed using the following formula (Brumsack, 2006):

$$element_{EF} = (element/Al)_{samp} \Big/ (element/Al)_{AS} \tag{1}$$

where $(element/Al)_{samp}$ is the ratio between the element and aluminum content in a sample, and $(element/Al)_{AS}$ is the ratio between the element and aluminum abundance in the average shale. We consider an $element_{EF} > 3$ as a detectable enrichment and an $element_{EF} > 10$ a moderate to strong authigenic enrichment (e.g., Tribovillard et al., 2006; Algeo and Tribovillard, 2009). Similarly, we interpret an $element_{EF} < 0.7$ as a detectable depletion and an $element_{EF} < 0.1$ as a moderate to strong authigenic depletion. Element concentrations above “normal” detrital background are expressed as element excess ($element_{xs}$) using the following formula:

$$[element]_{xs} = [element]_{samp} - (element/Al)_{bg} \times [Al]_{samp} \tag{2}$$

where $(element/Al)_{bg}$ was selected as the lowest element/Al ratio in the dataset (Brumsack, 2006; Meinhardt et al., 2016). Element/Al background values used to estimate excess concentrations for Mn, Si and Ba are reported in Table 1.

To evaluate the potential influence of carbonate dilution and normalization choice, we additionally tested carbonate-free Al normalization and Ca-normalized element excesses following approaches proposed for carbonate-rich successions (e.g., Jenkyns et al., 2017). The results of the various normalization procedures (see Supplementary Material) yield consistent stratigraphic patterns and long-term trends, demonstrating that the observed variations are not artifacts of normalization but reflect genuine changes in sedimentary inputs and environmental conditions. We further note that Al is not present at trace levels in the studied section, with Al_2O_3 concentrations consistently exceeding 0.5 wt%, well above analytical detection and quantification limits. While Al-based normalization may amplify short-scale variability in

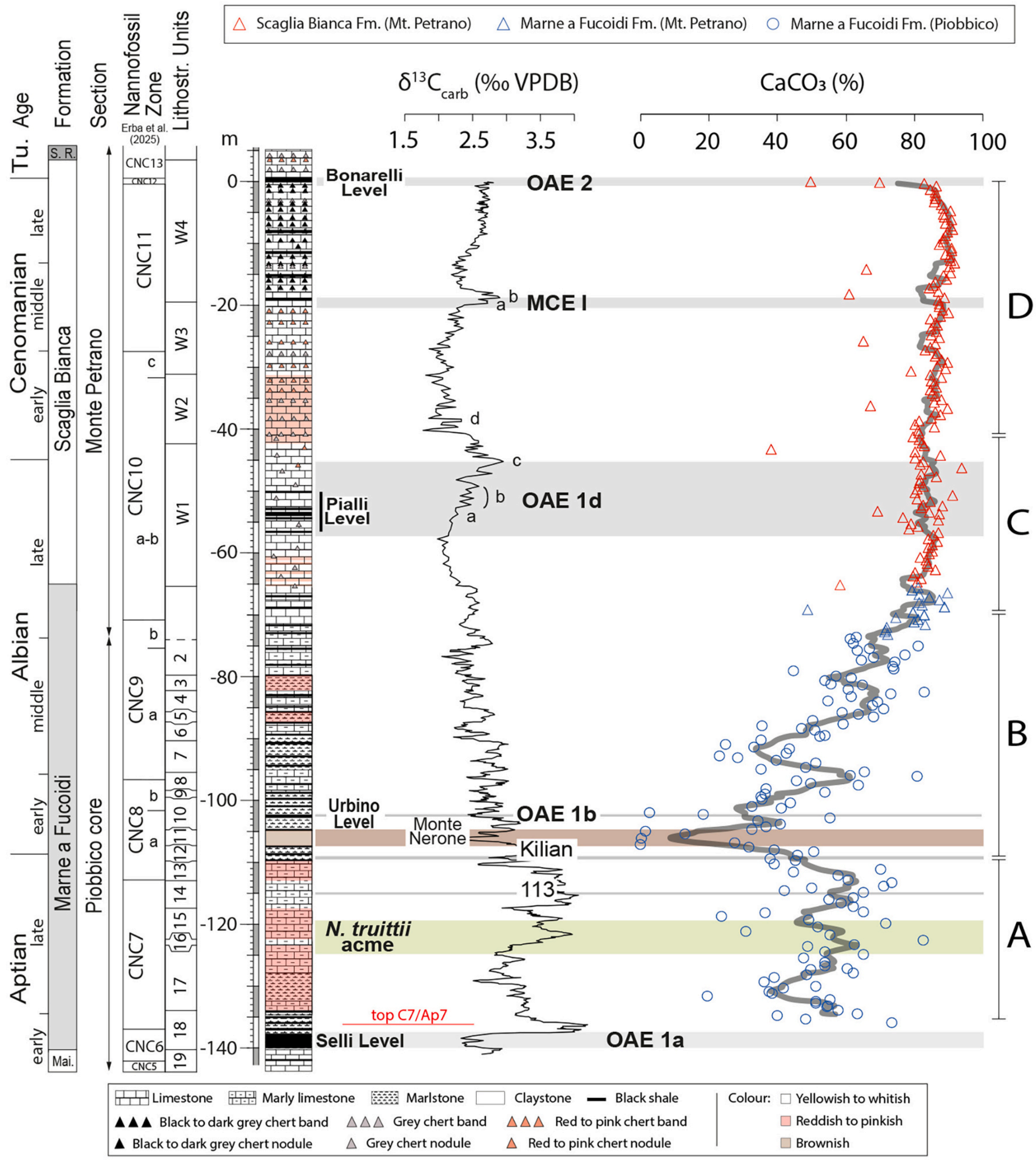

Fig. 3. From left to right: nannofossil biostratigraphy (Erba, 1988; Tiraboschi et al., 2009; Gambacorta et al., 2015; Bottini et al., 2015 – biozonation follows Erba et al., 2026); lithostratigraphic units (Marne a Fucoidi Fm. after Erba, 1988; Scaglia Bianca Fm. after Coccioni et al., 1992 and Coccioni and Galeotti, 2003); simplified lithologic log (Erba, 1988, 1992; Tornaghi et al., 1989; Gambacorta et al., 2015, 2016); $\delta^{13}C$ data from the (i) Piobbico Core (Tiraboschi et al., 2009; Erba et al., 2015) and (ii) Monte Petrano section (Giorgioni et al., 2012; Gambacorta et al., 2015); $CaCO_3$ content; radiolarian layers occurrence. Data from the Monte Petrano section are represented by open red and blue triangles for the Scaglia Bianca Fm. and Marne a Fucoidi Fm., respectively. Piobbico Core samples from the Marne a Fucoidi Fm. are represented by open blue circles. In grey is reported the 5-point moving average of reconstructed carbonate content values. To avoid artifacts, samples with $CaCO_3$ values lower than 45% in the Scaglia Bianca Fm. were not used for the 5-point moving average curve. (For interpretation of the references to colour in this figure legend, the reader is referred to the web version of this article.)

high-carbonate systems, this effect primarily affects minor point-to-point fluctuations and does not influence the overall stratigraphic signal discussed here. To minimize the influence of such short-term variations, a 5-point moving average was applied to the geochemical records, and interpretations are based exclusively on long-term trends.

Calcium carbonate content of analyzed samples was estimated using the following formula:

$$CaCO_3\ (\%) = [CaO_{xs}] \times \frac{100.0869\ amu}{56.0774\ amu} \tag{3}$$

where 100.0869 amu and 56.0774 amu are the molecular weights of $CaCO_3$ and CaO, respectively.

Following Hetzel et al. (2006) we use here a “Weathering Intensity” (WI) index defined as follows:

$$\text{Weathering Intensity (WI)} = \frac{[Al2O3]}{\sum detrital} \times 100 \tag{4}$$

where

Table 1
Background values for Ca/Al, Mn/Al, Si/Al, and Ba/Al. Ba/Al ratios are expressed as $\times 10^{-4}$. An asterisk marks those values that deviate from the average shale composition, reflecting local variations.

Local background	
(Element/Al)bg	
Ca/Al	* 0.13
Mn/Al	* 25
Si/Al	3.11
Ba/Al	* 12

$$\sum detrital = SiO_{2det} + TiO_2 + Al_2O_3 + Fe_2O_3 + MgO + MnO + CaO_{det} + K_2O + Na_2O + P_2O_5 \quad (5)$$

with SiO_{2det} and CaO_{det} calculated by subtracting the excess concentrations from the total concentrations of SiO_2 and CaO, respectively.

The WI index represents the amount of Al_2O_3 in the total detrital fraction normalized to 100%. Assuming that Al_2O_3 accumulates as a residual phase during prolonged chemical weathering, its increasing concentration relative to other detrital components – as reflected by higher WI index – indicates more intense weathering. Variations in the WI index may partly reflect changes in the lithology of the eroded source rocks; however, the large size of the sediment-routing system and the effective mixing of sediments likely reduce this influence, allowing WI index trends to be mainly attributed to basin-scale changes in chemical weathering intensity.

4. Results

4.1. Calcium carbonate content

The $CaCO_3$ values show significant variations from the Aptian to the uppermost Cenomanian (Fig. 3). Within the Marne a Fucoidi three major intervals are detected: 1) the upper Aptian up to just below the Kilian Level with ca. 55% $CaCO_3$ content; 2) from the Kilian Level to about 5 m below the Scaglia Bianca Fm. the average $CaCO_3$ is ca. 45% varying between 20 and 65% and few samples up to 80%, and the $CaCO_3$-poor Monte Nerone Level (0–20%); and 3) the uppermost ca. 5 m of the Marne a Fucoidi Fm. with higher $CaCO_3$ between ca. 70% to ca. 85%. In the Scaglia Bianca Fm. the $CaCO_3$ reaches ca. 85% (Fig. 3) and remains mostly constant up to the base of the Bonarelli Level.

4.2. Elemental data

Average major and trace element concentrations, element/Al, standard deviation (1 σ), maximum values and enrichment factors based on average shale (AS) values (Wedepohl, 1971, 1991) are reported in Table 2. Analyzed samples are on average enriched in P_2O_5 (EF = 7.5) and Cu (EF = 4.1) and strongly enriched in Ca (EF = 322.1), Ba (EF = 55.1), Mn (EF = 35.3), and Sr (EF = 19.1). On average, no depletion in any of the considered elements was observed. Enrichment factors for samples from the the Marne a Fucoidi and Scaglia Bianca are separately reported in Fig. S1 in the Supplementary Material. The Scaglia Bianca limestones are characterized by greater enrichments in CaO (EF = 534.2) and Sr (EF = 31.2) with respect to the Marne a Fucoidi lithologies. Furthermore, the Scaglia Bianca samples present higher enrichments also for Ba (EF = 66.8), P_2O_5 (EF = 10.8), and MnO (EF = 45.1).

4.3. Stratigraphic trends in elemental composition

The stratigraphic variation in Al_2O_3, Ti/Al, K/Al, WI index, and Mn_{xs} is reported in Fig. 4. Al_2O_3 concentrations are higher in the Marne a Fucoidi Fm., with values higher in the lower–middle Albian interval than in the reddish-greenish Aptian part. Concentrations then progressively decrease to low values reaching stable low values starting from ∼ − 72 m up to the base of the Bonarelli Level. The Ti/Al ratio is relatively uniform and remains below AS values, with relatively higher values in the interval above the top of isotopic segment C7/Ap7 up to about −117.5 m in correspondence of the reddish limestones of the Aptian interval. K/Al ratios remain largely stable and close to that of the average shale (AS) levels throughout the entire studied interval, except for a notable increase within the previously mentioned Aptian reddish limestone interval. The WI index shows higher values in the Aptian–lower Albian record (from the top isotopic segment C7/Ap7 to ∼ − 90 m), followed by a slight decrease up to ∼ − 72 m. Above this level, values are generally lower. The stratigraphic variation in Mn_{xs} concentrations along the studied record is marked by higher values in the Aptian–lower Albian interval (up to ∼ − 95 m), except for a decrease

Table 2
Average major and trace elements measured values of analyzed samples from the Monte Petrano section and Piobbico Core. All oxides are reported as %, minor and trace elements in μg/g. All trace element/Al and Mn/Al ratios are expressed as $\times 10^{-4}$. Average elements and element/Al standard deviations (1 σ), maximum values and enrichment factors (EF) are shown. EFs were calculated using average shale (AS) values from Wedepohl (1971, 1991), while EFs with an asterisk were estimated using local background concentrations reported in Table 1.

All samples (n = 281)								Monte Petrano and Piobbico Core		
Element	conc.	stand. Dev.	max	Average Shale	Element/Al	ratio	stand. Dev.	Average Shale		EF
SiO2	22.8	13.9	64.7	58.9	Si/Al	8.70	6.57	3.11		2.8
TiO2	0.14	0.13	0.56	0.78	Ti/Al	0.048	0.003	0.053		0.9
Al2O3	3.4	3.0	13.3	16.7	–	–	–	–		1.0
Fe2O3	1.4	1.3	6.4	6.9	Fe/Al	0.55	0.08	0.55		1.0
MgO	0.9	0.6	2.7	2.6	Mg/Al	0.39	0.14	0.18		2.2
CaO	38.6	11.4	52.7	2.2	Ca/Al	40.59	35.61	0.18 (*0.13)	*	322.1
Na2O	0.3	0.3	1.1	1.6	Na/Al	0.12	0.05	0.13		0.9
K2O	0.8	0.8	3.4	3.6	K/Al	0.37	0.03	0.34		1.1
P2O5	0.05	0.02	0.16	0.16	P/Al	0.023	0.013	0.008		7.5
Ba	929	770	3529	580	Ba/Al	661	541	66 (*12)	*	55.1
Cr	22	19	95	90	Cr/Al	14	7	10		1.4
Cu	29	40	413	45	Cu/Al	20.6	31.4	5.1		4.1
MnO	0.12	0.08	0.44	0.11	Mn/Al	882	642	96 (*25)	*	35.3
Ni	29	41	434	68	Ni/Al	16.4	8.5	7.7		2.1
Rb	29	25	109	140	Rb/Al	17	3	16		1.1
Sr	480	124	749	300	Sr/Al	651	588	34		19.1
V	28	17	87	130	V/Al	24	14	15		1.6
Y	16	8	38	41	Y/Al	13.4	6.4	4.6		2.9
Zn	33	34	458	95	Zn/Al	24	13	11		2.2
Zr	31	27	114	160	Zr/Al	18	3	18		1.0

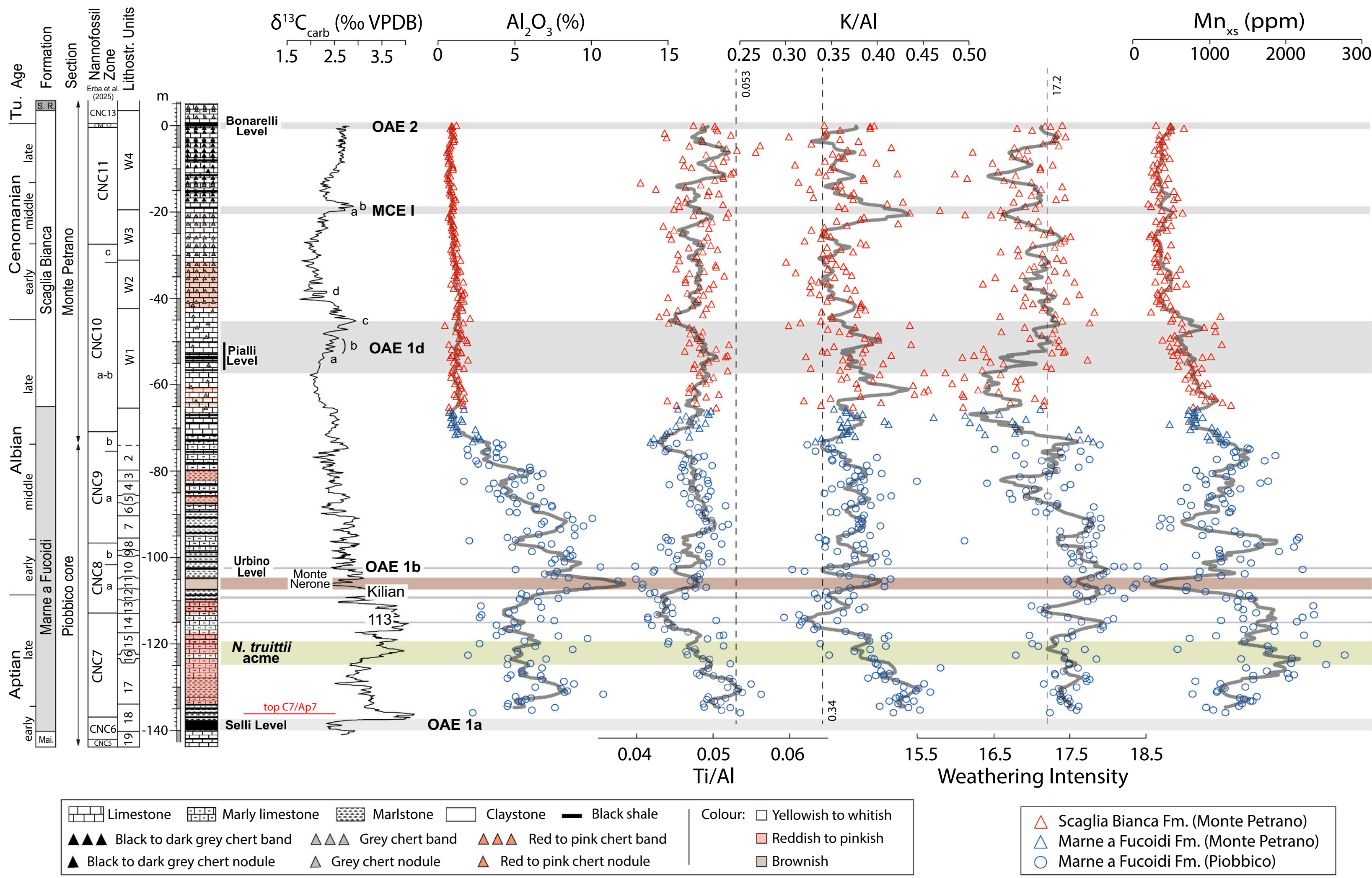

Fig. 4. Elemental data for the Monte Petrano section and Piobbico Core composite record. Data and smoothed curves based on a 5-point moving average of Al_2O_3, Ti/Al, K/Al elemental ratios, Weathering Intensity, and Mn_{xs} concentrations (this work). Samples from the Monte Petrano section are represented by open red and blue triangles for the Scaglia Bianca Formation and Marne a Fucoidi Formation, respectively. Piobbico Core samples from the Marne a Fucoidi Formation are represented by open blue circles. In grey is reported the 5-point moving average of each elemental ratio. The vertical line in the Ti/Al and K/Al graphs represents average shale (AS) composition according to Wedepohl (1971, 1991). The vertical line in the Weathering Intensity graph represents the average value of the studied record. For the sake of readability two samples with Ti/Al values greater than 0.058 were not reported in the figure and not used for estimating the 5-point moving average curve. Similarly, one sample with a Mn/Al value greater than 3000 was not considered during the estimate of the 5-point moving average curve. Lithostratigraphy, biostratigraphy, and chemostratigraphy as in Fig. 3. (For interpretation of the references to colour in this figure legend, the reader is referred to the web version of this article.)

around the Monte Nerone Level. After a brief decrease, concentrations increase again up to ~ – 74.5 m and then Mn_{xs} values progressively decline until ~ – 42.5 m (approximately at the boundary between members W1 and W2 sensu Coccioni and Galeotti, 2003), after which they stabilize at low values up to the base of the Bonarelli Level.

The stratigraphic variations in Si_{xs} and Ba_{xs} are reported in Fig. 5. Si_{xs} shows ample fluctuations (from ~ – 110.5 m to ~ – 70 m) in the Marne a Fucoidi Fm. with highest values in the following intervals: ~ – 110.5 m and – 100 m, between ~ – 94 m and – 87.5 m, and from ~ – 81 m to –72 m. In the Scaglia Bianca, Si_{xs} fluctuations are of lower amplitude with slightly elevated concentrations from ~ – 70 m to ~ – 41 m and before the onset of the Bonarelli Level (from ~ – 3.5 m to its base). Changes in Ba_{xs} exhibit a broadly similar, although not identical, trends to those of Si_{xs} with highest amplitude fluctuations between ~ – 110.5 m and ~ –71 m, marked by three intervals of elevated values: from ~ – 110.5 m and ~ 98.5 m, from ~ – 94 m and – 87.5 m, and from ~ – 81 m to –71 m. Additionally, the pre-Bonarelli increase in Ba_{xs} begins below the increase in Si_{xs}, at approximately –7 m.

5. Discussion

5.1. Sediment geochemistry

The studied lithologies consist of a mixture of three main components: biogenic carbonate, silica – which is mostly biogenic – and clay content. Relative variations in calcium carbonate, quartz and/or biogenic silica, and clays can be traced on a triangular diagram (Rachold and Brumsack, 2001) with axes CaO, SiO_2, and Al_2O_3 (Fig. S2 in the Supplementary Material). A straight line connecting the average shale composition to the CaO apex defines the so-called 'carbonate dilution line', which represents progressive dilution of an average shale-like detrital component by carbonate sedimentation. All samples plot below this line showing a shift toward higher SiO_2 content. This pattern suggests, for both formations, a homogeneous and stable background sedimentation dominated by varying proportions of carbonate and detrital clays, with a contribution from biogenic silica. Samples from the Scaglia Bianca Fm. cluster near the CaO vertex, as they consist

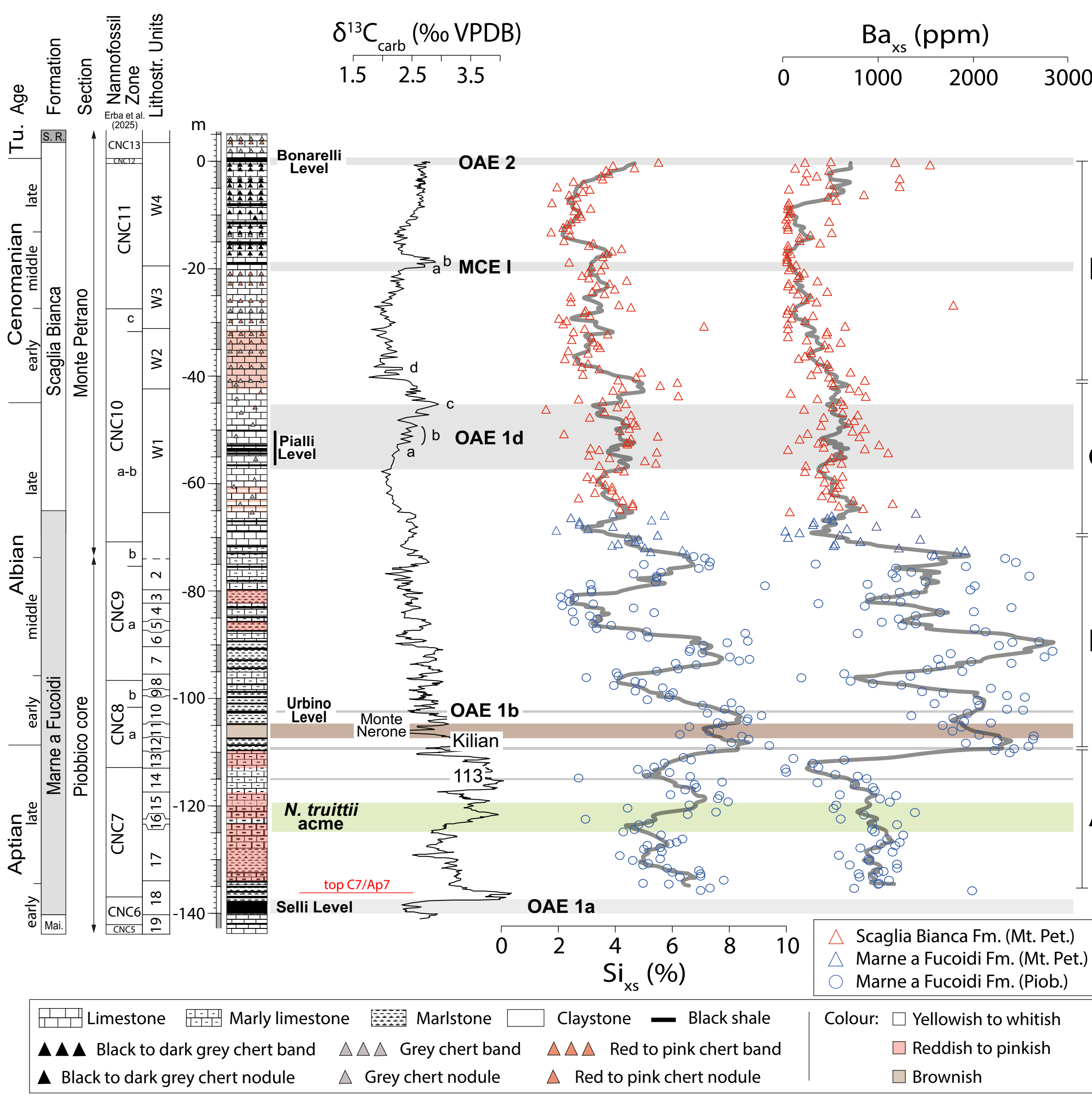

Fig. 5. Stratigraphic distribution of Sixs and Baxs concentrations for the Monte Petrano and Piobbico Core composite record. In grey is reported the 5-point moving average of the two elemental concentrations. For the sake of readability thirteen samples with Si_{xs} values greater than 10% were not reported in the figure and not used for estimating the 5-point moving average curve. Similarly, one sample with a Ba_{xs} concentration of about 1800 (at –26.7 m) was not used to compute the 5-point moving average curve. Lithostratigraphy, biostratigraphy, and chemostratigraphy as in Fig. 3.

predominantly of limestones, whereas most samples from the Marne a Fucoidi Fm. are shifted toward the AS point along the carbonate dilution line, indicating a persistent and variable detrital input. The Al_2O_3/TiO_2 ratio, used as an indicator of the original source rock composition (Garcia et al., 1994), has an average value of approximately 23.7, that points to a detrital source resembling the composition of the upper continental crust (Hayashi et al., 1997). Despite the abundance of biogenic silica in the Marne a Fucoidi Fm., as indicated by radiolarian-rich layers, chert occurrence is limited, likely because the relatively high clay content inhibited silica diagenesis. Experimental and field-based studies have shown that even small amounts of clay minerals, such as smectite, can significantly delay the transformation of biogenic silica to opal-CT and chert (Kastner et al., 1977; Williams et al., 1985). This interpretation is consistent with observations from deposits dominated by biogenic silica and characterized by very low detrital input, where rapid diagenetic transformation of biogenic silica is favored (Isaacs, 1982; Bohrmann et al., 1994).

Changes in the detrital fraction were estimated based on the elemental concentrations of Ti, K, Rb, and Zr, where Zr and Ti are used as indicators of the coarser to medium-sized detrital material (e.g., Cox et al., 1995; Schneider et al., 1997; Ganeshram et al., 1999; Sageman and Lyons, 2005), while Rb and K are associated with finer-grained particles, particularly aluminosilicates, K-feldspar, and clay minerals (Heinrichs et al., 1980; Cox et al., 1995; Calvert and Pedersen, 2007). When comparing TiO_2, K_2O, Rb, and Zr with Al_2O_3, their values are closely aligned with average shale (AS) values (Wedepohl, 1971, 1991), indicating no major changes in the bulk detrital geochemical composition, despite potential mineralogical variability (Fig. S3 in the Supplementary Material). In contrast, the SiO_2 versus Al_2O_3 plot (Fig. S3A in the Supplementary Material) shows most samples lying above the AS line, implying an additional input, from biogenic silica, besides the detrital background. These lithogenic element variations suggest a relatively stable detrital source over time in a low-energy, pelagic depositional environment.

Even if the detrital component remains compositionally stable through time, stratigraphic variations highlight significant changes in its relative abundance. The long-term trends in Al_2O_3 can be used as a proxy for the aluminosilicate fraction of the sediments, given that feldspar contents are negligible in the studied sedimentary rocks and that Al_2O_3 is only weakly affected by diagenesis (Brumsack, 1989; Calvert and Pedersen, 1993; Morford and Emerson, 1999; Wehausen et al., 2003; Piper and Perkins, 2004; Tribovillard et al., 2006; Zimmerli et al., 2024). The presence of an average of ~5.5 wt% Al_2O_3 in the upper Aptian interval of the Marne a Fucoidi Formation (Fig. 4) indicates the occurrence of some detrital input. These values are accompanied by relatively elevated Ti/Al and K/Al ratios, which may point to a contribution from aeolian dust (Schnetger, 1992; Schnetger et al., 2000; Wang et al., 2017). Such geochemical signatures are consistent with the composition of present-day Saharan dust, which is commonly enriched in Ti as a result of grain-size sorting processes typical of aeolian transport (Moreno et al., 2006; Muhs et al., 2010; Guinoiseau et al., 2022). In this context, the absence of sedimentological evidence for volcanic ash layers suggests that a volcanic contribution to the detrital component is unlikely. The hypothesis of an aeolian input appears consistent with climatic reconstructions at both regional and broader scales, which suggest a phase of increased aridity interrupted by humid interludes. On a broader regional scale, evaporitic layers identified in the Sorrento Peninsula (southern Italy) document Aptian episodes of arid hydroclimatic conditions alternating with wetter phases, which have been attributed to latitudinal shifts of tropical climate belts across the Tethys Ocean (Graziano and Raspini, 2015). The same authors also reported a transition from arid to more humid conditions across the equivalent of the 113 Level, which shows a decrease in Ti/Al and K/Al ratios around the equivalent stratigraphic interval in the Marne a Fucoidi Fm. On a supra-regional scale, further support for a semi-arid late Aptian climate is provided by palynological data and sedimentary evidence from the Algarve Basin (SW Portugal) (Heimhofer et al., 2008) and windblown desert sands in the Iberian Basin (Spain) (Rodríguez-López et al., 2006). A semi-arid climate characterized by a mixed aeolian and riverine contribution is also compatible with the relatively low global temperatures documented for the late Aptian time interval (Weissert and Lini, 1991; Mutterlose et al., 2009; Millán et al., 2014; McAnena et al., 2013; Bottini et al., 2015; Rodríguez-López et al., 2016; Bottini and Erba, 2018). Therefore, it is plausible that the geochemical signal recorded in the upper Aptian portion of the Marne a Fucoidi reflects some contribution to the detrital component from intensified wind activity under predominantly cool and semi-arid climatic conditions.

The Albian interval of the Marne a Fucoidi, instead, presents a rise in Al_2O_3 concentrations, with values higher than the Aptian interval. Although detrital input in this pelagic setting is limited, the lack of increase in Ti/Al and K/Al and the strong correlation between Al and all other detrital proxies (i.e., Si, Ti, Zr, K, and Rb) suggests the transport of a homogeneous terrigenous component lacking the grain-size sorting typically observed in aeolian deposits (Schnetger, 1992; Schnetger et al., 2000; Wang et al., 2017), indicating that riverine processes, rather than wind transport, are the primary source of the terrigenous material. A progressive decline in Al_2O_3 concentrations occurs few meters (ca. 5 m) below the base of the Scaglia Bianca Fm., leading to low and relatively stable values throughout the upper part of the record. This decrease reflects a drastic reduction in detrital supply, which is mirrored by an increase in $CaCO_3$ (Fig. 3), consistent with a phase of extremely limited runoff and a shift toward more carbonate-dominated sedimentation.

The variation in the WI index (Fig. 4) indicates that the degree of chemical weathering affecting the source material varied significantly through time. The pelagic depositional setting and the large distance from continental sources imply that the clay fraction reaching the basin was derived from well-mixed, distal detrital inputs. Although different clay minerals may experience selective retention during transport—kaolinite being a typical example of a phase preferentially trapped in more proximal environments (e.g., Thyberg et al., 2000)—the persistently distal setting suggests that such effects were broadly uniform through time. Consequently, the detrital material delivered to the basin was likely characterized by a relatively stable clay-mineral signature, systematically depleted in proximal phases. Under these conditions, the observed geochemical variability, and in particular the relative enrichment in Al captured by the WI index, is interpreted to predominantly reflect changes in the intensity of chemical weathering in the source areas rather than shifts in clay-mineral assemblages. During the late Aptian–early Albian interval, higher WI index values point to more intense weathering, whereas from the late Albian to the late Cenomanian the weathering intensity generally decreased. Notably, WI index values are relatively high during the Aptian interval, when other proxies suggest arid conditions. This apparent discrepancy implies that the Aptian climate was not persistently arid, but rather semi-arid, alternating phases of marked aridity with more humid intervals sufficient to sustain chemical weathering. The elevated WI index values recorded up to the lower upper Albian are consistent with enhanced weathering under more humid conditions, in agreement with the relative increase of detrital input to the basin. By contrast, during the Cenomanian, a marked drop in WI index values reflects a pronounced reduction in weathering intensity under climatically stable and arid conditions associated with the transition to the deposition of the limestones of the Scaglia Bianca Fm.

These major shifts in climatic conditions are supported by the palaeoclimate reconstructions of Burgener et al. (2023) and, more recently, by Scotese et al. (2025). According to these studies, during the Aptian the investigated site was located close to areas dominated by more arid conditions, possibly alternating phases of limited precipitation and short humid episodes. In contrast, during the Albian the Umbria-Marche Basin experienced a dominant and expanded equatorial humid belt, indicative of sustained high rainfall and more intense hydrological activity, consistent with the high detrital input observed in the Marne a Fucoidi Fm. In the Cenomanian, the palaeoclimate shifted again, with the onset of a broader subtropical arid belt and a reduction in rainfall. These reconstructions align well with the geochemical data, supporting the interpretation of a strong climatic control on the varying terrigenous fluxes during the Aptian–Cenomanian interval.

5.2. Controls on Mn_{xs} variability and provenance

In the studied record Mn concentrations exhibit marked fluctuations, which are especially pronounced within the Marne a Fucoidi Fm. In marine environments, Mn input can be influenced by several factors including riverine input, aeolian dust deposition, hydrothermal activity, and eustatic sea-level variations (Shiller, 1997; Corbin et al., 2000; Tribovillard et al., 2006; Mendez et al., 2010; Zhang et al., 2015; van Hulten et al., 2017).

Geochemical evidence of volcanism around OAE1b at Poggio le Guaine in the Umbria-Marche Basin (Sabatino et al., 2018; Matsumoto et al., 2020), suggest a brief interval of potential hydrothermal activity. Although Turgeon and Brumsack (2006) proposed a potential hydrothermal contribution to explain the Zn enrichment in the upper Cenomanian of the Furlo section, no significant enrichment in elements typically linked to hydrothermal processes (e.g., Si, Fe, Cu, Zn, Ni; Calvert and Pedersen, 2007) are detected, thus implying that Mn_{xs} variability was not of hydrothermal origin (Fig. 4).

Although sea-level changes could affect Mn delivery by altering the distance from continental sources (Elderfield, 1976; Aguilar-Islas and Bruland, 2006), the studied section was deposited at palaeodepths of ~1500–2000 m, where such variations would have minimal impact on proximity to the coast. Therefore, the observed Mn fluctuations must reflect other factors.

Aeolian input is unlikely to represent a major source of Mn, as it cannot account for the high Mn concentrations observed in the studied record. The composition of present-day Saharan dust is not enriched in Mn (Moreno et al., 2006; Muhs et al., 2010; Guieu et al., 2002), making aeolian supply an implausible explanation for the observed Mn excesses.

Nonetheless, diagenetic processes and redox conditions must also be considered, as Mn is highly sensitive to changes in bottom-water oxygenation (Pedersen and Price, 1982; Brumsack, 1986, 1989; Rajendran et al., 1992; Calvert and Pedersen, 1993, 1996; Morford et al., 2001; Cruse and Lyons, 2004; Tribovillard et al., 2006). Mass-balance calculations (Rachold and Brumsack, 2001) suggest that diagenetic redistribution of Mn through redox processes cannot account for the elevated Mn concentrations observed in the studied record. If both black shales and limestones are assumed to receive detrital inputs with an AS-like Mn composition, black shales could only act as temporary Mn reservoirs, later releasing Mn into adjacent carbonate sediments during early diagenesis. However, the Mn concentrations measured in the carbonates are substantially higher than those that could be supplied by the thin black shale intervals present in the stratigraphic record. A simple mass-balance consideration indicates that, to account for the observed Mn enrichments solely through redistribution, the cumulative thickness of Mn-rich black shales would need to exceed that of the carbonate intervals by several times. Such a requirement is clearly inconsistent with the observed stratigraphy. Therefore, even assuming efficient redox-driven Mn transfer, diagenetic redistribution alone cannot explain the Mn enrichments, implying the contribution of an additional Mn source. An exception is the Monte Nerone Level, where enhanced carbonate dissolution (Arthur and Premoli Silva, 1982; Erba, 1992) may have diagenetically reduced Mn_{xs} values, masking the actual input signal.

Based on the above considerations, fluvial input is regarded as the most plausible mechanism responsible for the elevated Mn concentrations observed in the studied succession. Although dissolved Mn^{2+} released by rivers is typically oxidized and rapidly precipitated under oxic conditions near river mouths, Mn can be efficiently redistributed under specific redox conditions. In particular, Mn transport may result from redox cycling occurring at or near the sediment–water interface, whereby intermittently reducing bottom-water conditions—documented by the occurrence of black shales—promote the reductive dissolution of Mn oxides at shallower sites, followed by basinward transfer of dissolved Mn and subsequent reprecipitation under more oxic conditions. Through repeated redox-driven dissolution–precipitation cycles, Mn can thus be progressively transferred from proximal source areas toward deeper portions of the basin. Alternatively, Mn could have been transported laterally within the water column along the oxygen minimum zone (OMZ), which acted as a pathway facilitating basinward transport of dissolved Mn away from the continental margin. Importantly, this process does not require an exceptionally expanded OMZ; observations from modern oceanic systems, such as the Pacific Ocean, demonstrate that even a normal OMZ can sustain Mn transport over considerable distances (Klinkhammer and Bender, 1980; Klinkhammer et al., 1997; Klinkhammer and McManus, 2001; Klinkhammer et al., 2009).

The elevated Mn_{xs} content observed in the Aptian reddish–greenish interval, even under conditions of reduced runoff and lower riverine Mn delivery relative to the Albian, is best explained by more efficient Mn retention linked to bottom-water redox conditions and early diagenetic processes. The red and green carbonates likely formed under oxic to mildly suboxic conditions, which favored the precipitation of Mn oxides and their incorporation into the carbonate lattice during early diagenesis. This mechanism accounts for the very high Mn values characteristic of the interval, despite a diminished but still active fluvial Mn supply. With the onset of Albian black-shale deposition, bottom-water conditions became cyclically more reducing. Under such conditions, Mn oxides were reduced to soluble Mn^{2+}, promoting partial Mn loss from the sediment. Nevertheless, carbonates interbedded with black shales still display relatively high Mn concentrations, indicating that bottom-water redox conditions oscillated between oxic and suboxic/anoxic states. Such oscillations allowed episodic re-oxidation and re-precipitation of Mn, implying the operation of a cyclic redox mechanism. Additional Mn may also have been locally mobilized from adjacent black-shale layers and reincorporated into the carbonates during early diagenesis. In summary, although Mn supply during the Aptian was lower than during the Albian due to reduced runoff, more efficient Mn fixation under predominantly oxic to mildly suboxic conditions characterized the reddish–greenish interval, whereas enhanced Mn escape under more reducing conditions characterized the Albian black shale–marlstone interval. In all cases, Mn availability remained primarily controlled by fluvial input, with redox conditions exerting a secondary control on Mn preservation. This is further proven by the good correlation between Mn_{xs} and Ca_{xs} in the reddish-greenish interval with respect to the black shale–marly limestone interval in the Albian, with R^2 values of ~0.71 and ~ 0.55, respectively (p-values equal to $\sim 2.25 \times 10^{-15}$ and $\sim 1.11 \times 10^{-14}$, respectively) (Fig. S4 in the Supplementary Material). Finally, an additional Mn contribution—beyond that supplied by rivers—during the deposition of the Marne a Fucoidi Fm. cannot be excluded. Reducing sediments from shelfal areas could have supplied dissolved Mn to deeper settings, as it occurs in modern oceans (e.g., in the Arabian Sea as discussed in Schnetger et al., 2000). Evidence for upwelling has been proposed, for example, in coeval sediments of the Western Tethyan Vocontian Basin by Bréhéret and Brumsack (2000).

In the uppermost part of the Marne a Fucoidi, the drastic decrease in Mn_{xs} to stable low values for the entire Cenomanian is associated with the disappearance of rhythmically interbedded black shales and characterized by limestones reflecting negligible runoff and minimal Mn supply under fully arid climatic conditions. The Cenomanian steady low Mn_{xs} concentrations can be divided into two segments: a lower part (Interval C, Fig. 4) where low values indicate a minimal fluvial input, and an upper part (Interval D, Fig. 4), reaching the base of the Bonarelli Level, where even lower values reflect an extremely limited runoff.

5.3. Palaeoproductivity fluctuations

The Si_{xs} and Ba_{xs} curves provide insights into relative productivity variations in the Umbria–Marche Basin during the studied interval. Although both proxies exhibit broadly similar large-scale trends, they display differences in magnitude and small-scale fluctuations, likely reflecting their distinct origins and depositional controls. Si_{xs} is commonly utilized as an indicator of trophic conditions (e.g., Schmitz et al., 1997; Turgeon and Brumsack, 2006; Hu et al., 2009), deriving from biogenic opaline silica. Ba_{xs} is considered an indicator of productivity (e.g., Dehairs et al., 1980; Brumsack and Gieskes, 1983; Brumsack, 1986, 1989; Dymond et al., 1992; McManus et al., 1998; Gingele et al., 1999; Babu et al., 2002; Paytan and Griffith, 2007; Schoepfer et al., 2015; Liguori et al., 2016) at sites with water depths greater than 1000 m (Babu et al., 2002) being associated with acantharians, a group of celestinite-secreting radiolaria involved in Ba uptake and barite formation (Bernstein et al., 1998; Bernstein and Byrne, 2004; Jacquet et al., 2007). Ba is a less reliable proxy for palaeoproductivity under reducing conditions, particularly in regions with intense sulfate reduction, as it becomes mobile (Brumsack and Gieskes, 1983; Dymond et al., 1992; Torres et al., 1996; Tribovillard et al., 2006), but this case does not account for the studied samples as they consist of limestones, marly limestones, and marlstones.

Relative variations in Si_{xs} and Ba_{xs} curves indicate that oligo–mesotrophic conditions prevailed during the late Aptian. At the Kilian Level, a pronounced increase in these proxies is observed, which persisted, with some fluctuations, through the lower–middle Albian, suggesting a transition from mesotrophic to locally eutrophic conditions. Oligo- to mesotrophic conditions developped in the late Albian and then declined to oligotrophy in the Cenomanian, before rising again just prior to the Bonarelli Level.

To further evaluate palaeoproductivity changes inferred from the geochemical proxies, the Si_{xs} and Ba_{xs} records were compared with the micropalaeontological Nutrient Index (NI) of Bottini and Erba (2018) for the same composite section. The NI is based on calcareous nannofossil data and is calculated as the ratio between mesotrophic taxa (*Biscutum constans, Zeugrhabdotus erectus* and *Discorhabdus ignotus*) and oligotrophic taxon (*Watznaueria barnesiae*).

The comparison is performed using smoothed curves (5-point moving average) of Si_{xs}, Ba_{xs}, and NI, and by distinguishing four broad trophic regimes: oligotrophic, oligo–mesotrophic, mesotrophic, and eutrophic (the latter not reached by the NI). On this basis, the long-term trends of the geochemical and micropalaeontological proxies show substantial agreement although with discrepancies. Differencies occur in three specific segments: in the *N. truittii* acme (classified as oligotrophic by the NI), in the Aptian/Albian boundary interval (predominantly oligotrophic in the NI but punctuated by mesotrophic peaks), and in the middle Albian (oligo-mesotrophic according to the NI) (Fig. 6). Part of the mismatches observed may be explained by the different bases of the proxies. The Ba and Si records reflect the productivity of siliceous

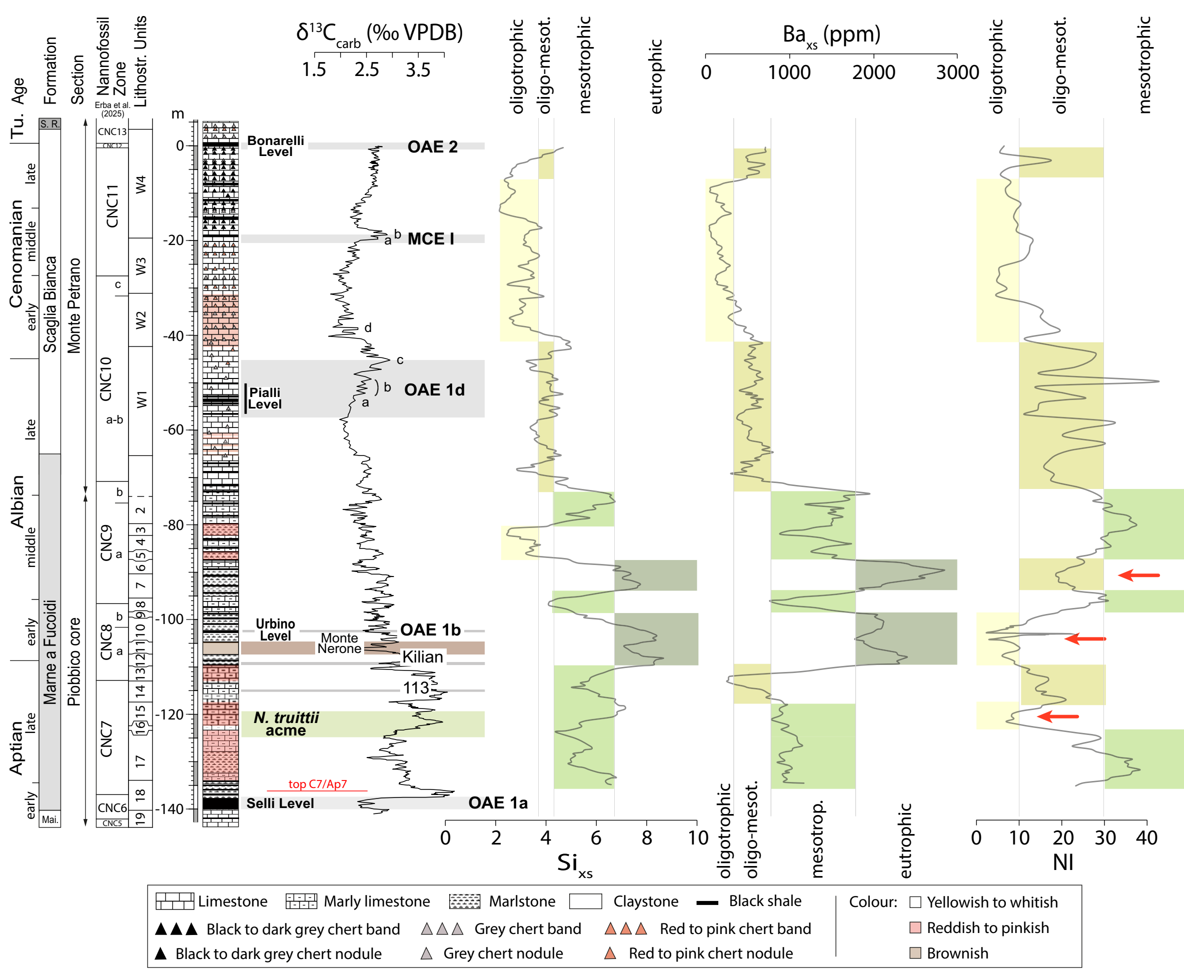

Fig. 6. Comparison of elemental-based estimates of palaeoproductivity conditions, based on Si_{xs} and Ba_{xs} concentrations, with the nannofossil nutrient index (NI) estimated for the same stratigraphic record by Bottini and Erba (2018). Colors highlight intervals interpreted as having different trophic levels. Red arrows indicate the three intervals where the NI curve is discrepant with the trends suggested by the elemental data. The original NI data from Bottini and Erba (2018) for the Piobbico Core were smoothed using a 5-point moving average. See text for details. (For interpretation of the references to colour in this figure legend, the reader is referred to the web version of this article.)

plankton which is typically associated with meso- to eutrophic environments whereas the NI is based on coccolithophores that preferentially thrive in oligotrophic to mesotrophic waters. As a result, the NI primarily reflects fluctuations within the oligotrophic–mesotrophic range and may fail to capture episodes of enhanced productivity that are instead highlighted by the geochemical proxies.

5.4. Environmental changes across the mid-Cretaceous in the Western Tethys

The dataset presented in this study suggests that the Western Tethys underwent pronounced environmental fluctuations in the late Aptian to the latest Cenomanian. Trends inferred from elemental proxies, together with nutrient and temperature variations derived from calcareous nannofossils (Bottini and Erba, 2018) allowed the identification of four intervals, labelled A to D, from the oldest to the youngest (Fig. 7). While mid-Cretaceous climate was characterized by a pronounced latitudinal zonation (e.g., Scotese et al., 2021), the variations documented here provide a detailed record of environmental changes in the Umbria–Marche Basin within the Western Tethys, offering insights into regional expressions of broader climatic trends.

5.4.1. Upper Aptian interval (a)

The upper Aptian portion of the Marne a Fucoidi, following the Selli Level, is characterized by oligo–mesotrophic conditions, generally low to moderate fluvial runoff and cooler climatic settings compared to both the early Aptian and the Albian. The semi-arid climate likely favored an increased aeolian contribution to sedimentation. Minimum temperatures were reached during the "Aptian Cold Snap," a globally recognized cooling phase (Weissert and Lini, 1991; Mutterlose et al., 2009; Millán et al., 2014; McAnena et al., 2013; Bottini et al., 2015; Rodríguez-López et al., 2016). The semi-arid conditions were punctuated by brief episodes of precipitations that provided sufficient moisture to sustain prolonged chemical weathering, even under relatively cooler temperatures (Sherman, 1952; Stallard, 1985; White and Blum, 1995; Maher, 2011; Ferrier et al., 2016). Indeed, in the nearby Belluno Basin, Bauer et al. (2024) documented that intensified weathering during OAE 1a continued for at least one million years after the termination of the Selli Level deposition. The record of the Marne a Fucoidi Fm. suggests that this weathering regime continued across the late Aptian although probably gradually decreasing its intensity under progressively drier conditions. These environmental conditions favored prevailing oligo- to oligo-mesotrophic surface water conditions, promoting oligotrophic taxa such as nannoconids during the *N. truittii* acme, and persistently well-oxygenated bottom waters as evidenced by dominant red lithologies.

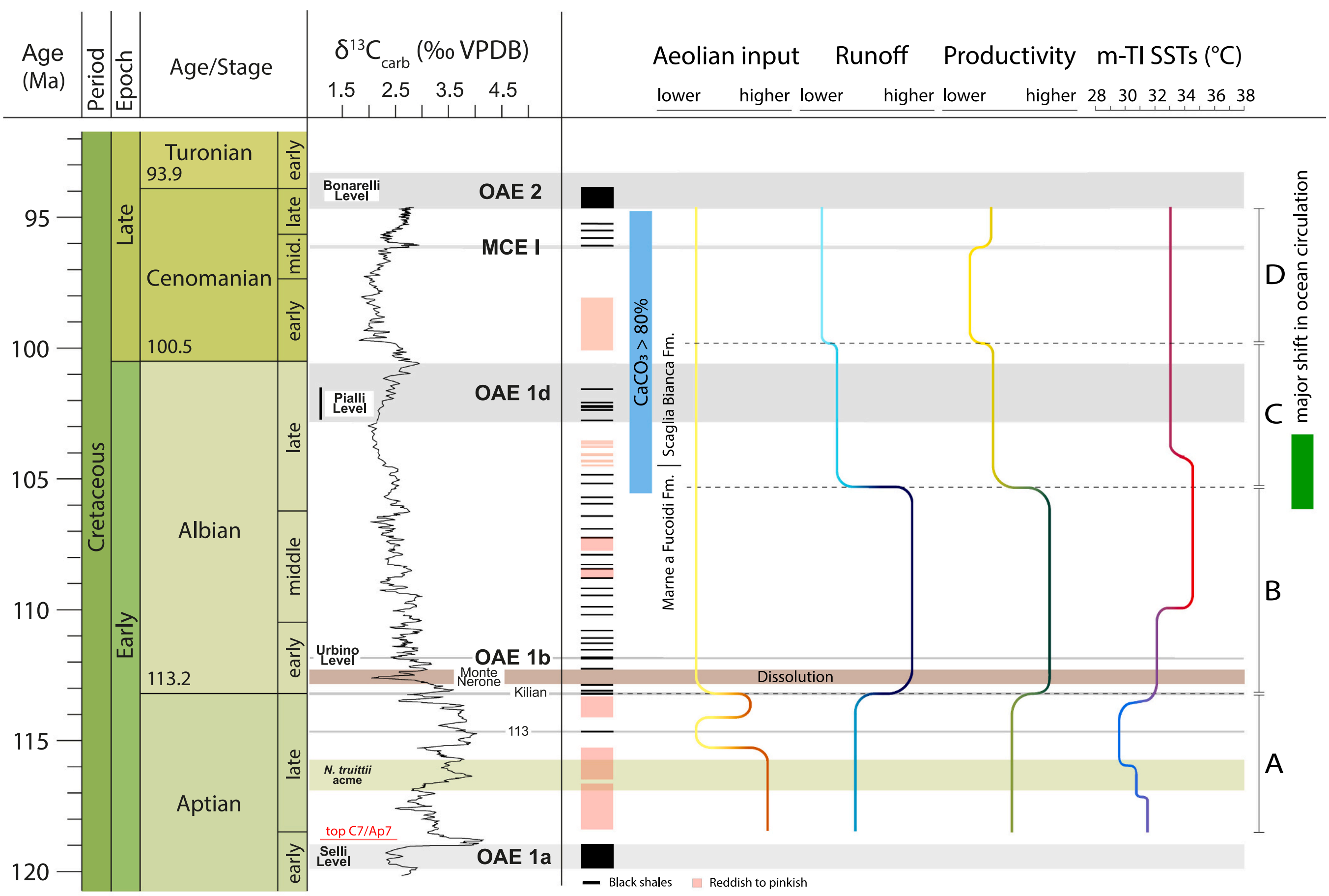

Fig. 7. Synthesis of elemental-based weathering, runoff, and palaeoproductivity variations in the Western Tethys during the mid-Cretaceous. A schematic lithological log is also provided, showing the occurrence of black shales and reddish-pinkish intervals, along with a blue bar indicating the interval above which $CaCO_3$ content exceeds 80%. Temperature variations are derived from the modified nannofossil temperature index (m-TI, °C), as reconstructed by Bottini and Erba (2018). Intervals A to D reported on the right side of the panel are defined and described in the text. The green bar indicates the approximate stratigraphic interval during which, according to Giorgioni et al. (2012, 2015), a major shift in ocean circulation occurred. Timescale is after Gradstein et al. (2020). See text for details. (For interpretation of the references to colour in this figure legend, the reader is referred to the web version of this article.)

5.4.2. Lowermost Albian–lower upper Albian interval (B)

Lithological and geochemical data, together with nutrient and temperature variations derived from calcareous nannofossils (Bottini and Erba, 2018), consistently indicate that a major climatic and oceanographic reorganization occurred at the Kilian Level (Interval B in Fig. 7; Fig. 8B). This shift is marked by the onset of a pronounced warming trend and an increase in surface-water fertility, coeval with a transition toward more humid climatic conditions. Although the basin remained fully pelagic, these changes are interpreted to have influenced nutrient availability at the basin scale. The establishment of a monsoon-like climate regime was proposed for both the Umbria–Marche Basin (Pratt and King, 1986; Giorgioni et al., 2012) and the Vocontian Basin (Herrle et al., 2003) during this time interval, pointing to climatically unstable conditions.

Giorgioni et al. (2015, 2017) postulated that the frequent fluctuations in oceanographic conditions during the Albian can be partly

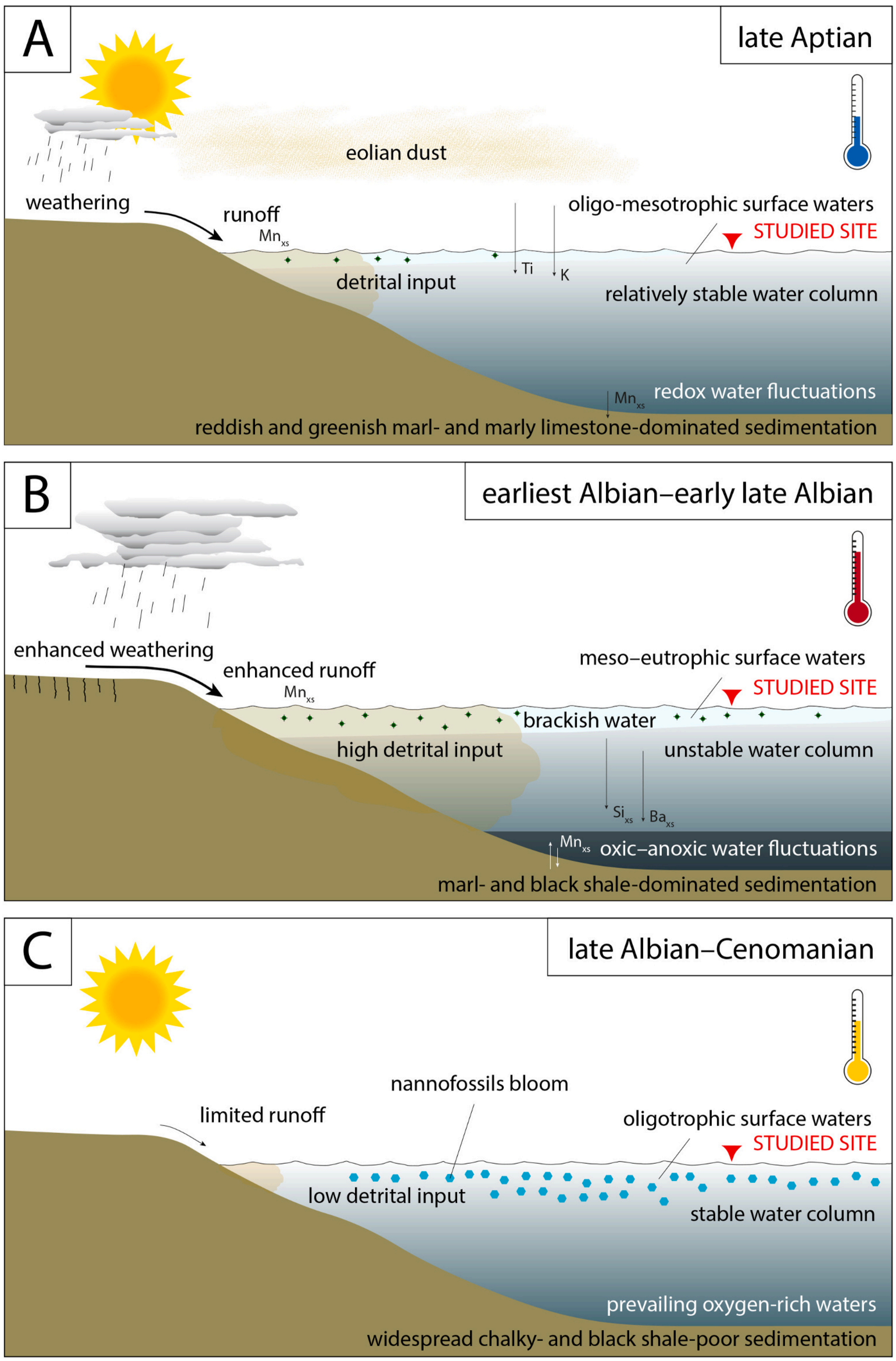

Fig. 8. Temporal and palaeogeographic variations in the Western Tethys and North Atlantic in the A) late Aptian (Interval A in Figs. 4, 5, and 8), B) earliest Albian–early late Albian (Interval B in Figs. 4, 5, and 8), and C) late Albian–Cenomanian (Intervals C and D in Figs. 4, 5, and 8).

attributed to the distinctive palaeogeographic configuration, characterized by an east–west oriented Tethys Ocean flanked by extensive continental masses. This configuration likely amplified the response of the regional hydrological cycle and ocean circulation to orbitally forced climate variability. In this context, repeated and intense rainfall events would have promoted weathering, increased fluvial runoff, and enhanced the flux of freshwater and nutrients into the basin.

The geochemical and micropalaeontological records together suggest that surface-water conditions oscillated between mesotrophic and eutrophic phases. Herbert et al. (1986) proposed that part of the nutrient-rich fluvial input may have originated from large tropical river systems draining African cratonic regions. The intermittent influx of freshwater, rich in nutrients and suspended sediments, would have triggered rhythmic enhanced surface productivity while also lowering surface salinity, strengthening the halocline and thermocline, thus enhancing water column stratification and limiting deep-water ventilation (Fig. 8B).

Notably, the reddish intervals of the Albian differ from those of the upper Aptian. While the cooler late Aptian conditions promoted the delivery of cold, oxygen-rich waters to the seafloor, the warmer Albian temperatures resulted in the deposition of red units due to downwelling of warm, more saline, nutrient-depleted tropical waters characterized by relatively high oxygen content (Grippo et al., 2004). Generally warm conditions developed a reorganization of the ocean circulation with shifts in downwelling zones (Herrle, 2002).

5.4.3. Upper Albian–Cenomanian interval (C and D)

The upper Albian to Cenomanian interval (Intervals C and D in Fig. 7; Fig. 8C) records a shift toward moderately warm temperatures and arid climatic conditions, resulting in a weakened hydrological cycle, reduced chemical weathering, and negligible continental runoff. The sharp decline in fluvial input and nutrient delivery to marine environments was responsible for a decrease in fertility associated with well-oxygenated bottom waters. These conditions mirror those observed in modern oligotrophic oceanic areas, where nutrient limitation favors calcareous nannoplankton proliferation, ultimately boosting carbonate production (Premoli Silva et al., 1999; Leckie et al., 2002; Erba, 2004; Gambacorta et al., 2016). Lithologically, this environmental change is reflected in the disappearence of black shales and an increase in $CaCO_3$ contents exceeding 80%. Black shales of the Pialli Level (middle part of Interval C) and following the MCE I (upper part of Interval D) are not associated to long-term variations in geochemical proxies. Indeed, as suggested by elemental productivity proxies and the nannofossil NI, a lower-magnitude increase in fertility occurred in correspondence with the interval directly preceding the Bonarelli Level (approximately 7 m below its base).

Although the lithostratigraphic boundary between the Marne a Fucoidi and the Scaglia Bianca is defined by the lowermost occurrence of chert nodules, the geochemical boundary between intervals B and C—marked by a decrease in the detrital fraction—occurs ca. 5 m below the lithostratigraphic boundary. As discussed above, chert formation requires the clay fraction to fall below a critical threshold, thus a lag of approximately 1 million years (based on Gradstein et al., 2020) is detetected between the onset of the geochemical changes (base of Interval C) and the lithostratigraphic base of the Scaglia Bianca Fm.

Interval C (Fig. 7) represents the transition in the pelagic Western Tethys from the unstable conditions of the early to early late Albian (Interval B) to the more stable regime of the Cenomanian (Interval D). Within this interval, a steady decline in Mn_{xs} concentrations points to decreasing runoff, paralleled by a shift from mesotrophic to progressively more oligotrophic conditions. Warm and arid conditions continued into the Cenomanian (Interval D in Fig. 7), further reinforcing oligotrophic surface waters under reduced runoff. Stable water column stratification, well-ventilated bottom waters resulted in widespread carbonate sedimentation.

According to Giorgioni et al. (2012, 2015), a major shift in ocean circulation occurred during the late Albian between the upper *Ps. ticinensis* and the *Th. appenninica* zones (Fig. 7), from an unstable regime marked by frequent fluctuations driven by orbital forcing to a more stable mode characterized by improved basin connectivity, persistent thermocline stratification, efficient current systems, and well-defined upwelling and downwelling zones. These changes collectively reduced the ocean system's sensitivity to orbital forcing. This transition is marked by a steady increase in carbonate content and the near disappearance of black shale layers, accompanied by the fading of orbital signals in $\delta^{13}C$ values. Giorgioni et al. (2015) supposed that the main driver of this transition was tectonic in nature. Several authors (Holbourn et al., 2001; Caus et al., 2009; Handy et al., 2010) suggested that the counterclockwise rotation of Iberia initiated during the Aptian progressively deepened the Betic–Gibraltar–Rifian gateways, leading to a significantly improved Atlantic–Tethyan connection by the Cenomanian. Such tectonic reorganization, coupled with a global sea-level rise that enhanced the connection between shallow and deep-water settings, promoted a more efficient circulation regime and improved basin ventilation. The stabilization of the Equatorial Circumglobal Current facilitated the onset of a supra-regional deposition of chalky-limy sediments in the latest Albian (Giorgioni et al., 2015). Our data are consistent with this hypothesis; however, we suggest that, in the studied area, changes in regional palaeoclimatic regimes played an instrumental role, as evidenced by shifts in weathering, terrigenous input, and nutrient recycling. Rather than acting independently, tectonic forcing and regional climate variability likely operated in concert, with tectonic reorganization setting the boundary conditions for gateway geometry and basin connectivity, thereby influencing large-scale circulation and ventilation patterns. While improved oceanic connectivity may have facilitated more efficient large-scale circulation, we propose that, in the studied basin, climate changes acted as co-driver of the oceanic reorganization. Indeed, as noted by Giorgioni et al. (2015), the onset of more stable conditions favored calcareous plankton and persistent bottom-water ventilation, resulting in widespread carbonate-rich sedimentation. However, we emphasize that this transition was driven by both enhanced pelagic micrite production and a marked reduction in terrigenous input under increasingly arid climatic conditions.

6. Conclusions

The geochemical record from the Piobbico Core - Monte Petrano composite section provides the first comprehensive reconstruction of the long-term environmental and climatic evolution in the Umbria-Marche Basin during the late Aptian to latest Cenomanian (~25 million years). Elemental data document a progressive environmental transition from the dynamic and climatically unstable conditions of the Marne a Fucoidi Fm. – characterized by alternating reddish, greenish, and black shale-rich intervals – to the more stable, oligotrophic conditions producing the carbonate-rich lithologies of the Scaglia Bianca Fm.

In the studied area, the late Aptian was marked by semi-arid, cooler conditions, predominantly oligo–mesotrophic surface waters, and oxygenated bottom waters with deposition of red facies. Starting at the Aptian/Albian boundary, a warming trend triggered enhanced weathering and intensified runoff associated with meso- to eutrophic conditions and stratified water-masses, which persisted in the basin through the middle Albian. During the late Albian, a major climatic and oceanographic reorganization occurred, triggering negligible terrigenous input, and occurring approximately 1 million years before the lithostratigraphic base of the Scaglia Bianca Fm. The onset of the Scaglia Bianca coincides with a moderate decrease in average temperatures, underscoring the crucial role of temperature in modulating depositional processes. The Scaglia Bianca Fm. reflects a regime of increasingly stable, warm, and arid conditions, which limited nutrient supply and productivity. The resulting oligotrophic conditions, combined with well-oxygenated bottom waters, favored the deposition in the Umbria-Marche Basin of carbonate-rich sediments through the Cenomanian until the onset of OAE 2.

The observed climatic evolution can be explained by latitudinal shifts in the position of major climatic belts relative to the Umbria–Marche Basin, particularly changes in the mean position of the Intertropical Convergence Zone (ITCZ) and the subtropical arid belts. During the cooler late Aptian phase, the basin was likely located under the influence of subtropical high-pressure systems, limiting precipitation and resulting in semi-arid conditions. During the earliest Albian to early late Albian interval, a northward displacement of the ITCZ and expansion of the associated monsoon-like circulation brought warm and humid conditions to the region, enhancing precipitation, runoff, and nutrient delivery. Subsequently, during the late Albian to late Cenomanian, although temperatures remained high, the mean position of the ITCZ shifted southward relative to the basin, while the subtropical arid belts expanded, leading to the renewed dominance of dry conditions and a shift to fully arid conditions associated with persistently warm temperatures.

Overall, our results emphasize the pivotal role of regional climate variability, expressed through temperature fluctuations and shifts between humid and arid conditions, in regulating depositional processes and shaping the palaeoenvironmental evolution in the Western Tethys. The transition from unstable, nutrient-rich environments to more stable oligotrophic regimes reflects broader reorganizations of the hydrological cycle, ocean circulation, and redox conditions in response to long-term regional climate change, operating within a tectonically evolving framework that modulated basin connectivity and circulation pathways.

CRediT authorship contribution statement

Gabriele Gambacorta: Visualization, Validation, Methodology, Investigation, Formal analysis, Conceptualization, Writing – review & editing, Writing – original draft. **Philipp Böning:** Validation, Methodology, Formal analysis, Writing – review & editing, Writing – original draft. **Hans-Jürgen Brumsack:** Validation, Investigation, Writing – review & editing, Writing – original draft. **Elisabetta Erba:** Funding acquisition, Conceptualization, Writing – review & editing, Writing – original draft. **Cinzia Bottini:** Writing – review & editing, Writing – original draft.

Declaration of competing interest

The authors declare that they have no known competing financial interests or personal relationships that could have appeared to influence the work reported in this paper.

Acknowledgments

This research was conducted within the PRIN 2017RX9XXXY awarded to EE and the Italian Ministry of Education (MIUR) project “Dipartimenti di Eccellenza 2018–2022, Le Geoscienze per la Società: Risorse e loro evoluzione” awarded to the University of Milan. The authors are grateful to both Jean-François Deconinck and an anonymous Reviewer whose valuable comments contributed greatly to improving the quality of the manuscript. We also thank the Editor, Haijun Song, for his constructive suggestions.

Appendix A. Appendices

Datasets related to this article can be found in the Dataverse Repository (https://doi.org/10.13130/RD_UNIMI/KQJPV7). The dataset consists of a table with major and trace element data for the Monte Petrano and Piobbico Core records. Seven additional figures are provided as Supplementary Material.

Appendix A. Supplementary data

Supplementary data to this article can be found online at https://doi.org/10.1016/j.gloplacha.2026.105414.

Data availability

The authors confirm that all data necessary for supporting the scientific findings of this paper have been provided.

References

Aguilar-Islas, A., Bruland, K., 2006. Dissolved manganese and silicic acid in the Columbia River plume. Mar. Chem. 101, 233–247.

Algeo, T.J., Tribovillard, N., 2009. Environmental analysis of paleoceanographic systems based on molybdenum–uranium covariation. Chem. Geol. 268, 211–225.

Alvarez, W., 1990. Pattern of extensional faulting in pelagic carbonates of the Umbria–Marche Apennines of Central Italy. Geology 18, 407–410.

Arthur, M.A., Premoli Silva, I., 1982. Development of widespread organic carbon-rich strata in the Mediterranean Tethys. In: Schlanger, S.O., Cita, M.B. (Eds.), Nature and Origin of Cretaceous Carbon-Rich Facies. Academic Press, London, pp. 7–54.

Arthur, M.A., Jenkyns, H.C., Brumsack, H.-J., Schlanger, S.O., 1990. Stratigraphy, geochemistry, and paleoceanography of organic carbon-rich cretaceous sequences. In: Ginsburg, R.N., Beaudoin (Eds.), Cretaceous Resources, Events and Rhythms: Background and Plans for Research. Kluwer, pp. 75–119.

Babu, C.P., Brumsack, H.-J., Schnetger, B., Böttcher, M.E., 2002. Barium as a productivity proxy in continental margin sediments: a study from the eastern Arabian Sea. Mar. Geol. 184 (3–4), 189–206.

Bauer, K.W., Bottini, C., Frei, R., Asael, D., Planavsky, N.J., Francois, R., McKenzie, N.R., Erba, E., Crowe, S.A., 2021. Pulsed volcanism and rapid oceanic deoxygenation during Oceanic Anoxic Event 1a. Geology 49, 1452–1456.

Bauer, K.W., McKenzie, N.R., Cheung, C.T., Gambacorta, G., Bottini, C., Nordsvan, A.R., Erba, E., Crowe, S.A., 2024. A climate threshold for ocean deoxygenation during the early cretaceous. Nature 633 (8030), 582–586.

Bernoulli, D., 1972. North Atlantic and Mediterranean Mesozoic facies: A comparison. In: Hollister, C.D., Ewing, J.I., et al. (Eds.), Initial Reports Deep Sea Drilling Project, 11. U.S. Government Printing House, Washington, D.C., pp. 801–879

Bernoulli, D., Jenkyns, H.C., 1974. Alpine, Mediterranean and Central Atlantic Mesozoic facies in relation to the early evolution of the Tethys. In: Dott Jr., R.H., Shaver, R.H. (Eds.), Modern and Ancient Geosynclinal Sedimentation, vol. 19. SEPM Special Publication, pp. 129–160.

Bernoulli, D., Jenkyns, H.C., 2009. Ancient oceans and continental margins of the Alpine-Mediterranean Tethys: deciphering clues from Mesozoic pelagic sediments and ophiolites. Sedimentology 56, 149–190.

Bernstein, R.E., Byrne, R.H., 2004. Acantharians and marine barite. Mar. Chem. 68, 45–50.

Bernstein, R.E., Byrne, R.H., Schijf, J., 1998. Acantharians: a missing link in the oceanic biogeochemistry of barium. Deep Sea Res. Pt. I 45, 491–505.

Blok, C.N., Ineson, J., Anderskouv, K., Fantasia, A., Sheldon, E., Thibault, N., Jelby, M.E., Adatte, T., Bodin, S., 2022. Latitude-dependant climate changes across the Aptian Oceanic Anoxic Event 1a. Palaeogeogr. Palaeoclimatol. Palaeoecol. 601, 111085.

Bodin, S., Meissner, P., Janssen, N.M.M., Steuber, T., Mutterlose, J., 2015. Large igneous provinces and organic carbon burial: Controls on global temperature and continental weathering during the early cretaceous. Glob. Planet. Chang. 133, 238–253.

Bodin, S., Charpentier, M., Ullmann, C.V., Rudra, A., Sanei, H., 2023. Carbon cycle during the late Aptian–early Albian OAE 1b: A focus on the Kilian–Paquier levels interval. Glob. Planet. Chang. 222, 104074.

Bohrmann, G., Abelmann, A., Gersonde, R., Hubberten, H., Kuhn, G., 1994. Pure siliceous ooze, a diagenetic environment for early chert formation. Geology 22, 207–210.

Bornemann, A., Erbacher, J., Heldt, M., Kollaske, T., Wilmsen, M., Lübke, N., Huck, S., Vollmar, N.M., Wonik, T., 2017. The Albian–Cenomanian transition and Oceanic Anoxic Event 1d – an example from the Boreal Realm. Sedimentology 64, 44–65.

Bottini, C., Erba, E., 2018. Mid-cretaceous paleoenvironmental changes in the western Tethys. Clim. Past 14, 1147–1163.

Bottini, C., Cohen, A.S., Erba, E., Jenkyns, H.C., Coe, A.L., 2012. Osmium-isotope evidence for volcanism, weathering, and ocean mixing during the early Aptian OAE 1a. Geology 40, 583–586.

Bottini, C., Erba, E., Tiraboschi, D., Jenkyns, H.C., Schouten, S., Sinninghe Damsté, J.S., 2015. Climate variability and ocean fertility during the Aptian Stage. Clim. Past 11, 383–402. https://doi.org/10.5194/cp-11-383-2015.

Bréhéret, J.-G., Brumsack, H.-J., 2000. Barite concretions as evidence of pauses in sedimentation in the Marnes Bleues Formation of the Vocontian Basin (SE France). Sediment. Geol. 130, 205–228.

Brumsack, H.J., 1986. The inorganic geochemistry of cretaceous black shales (DSDP leg 41) in comparison to modern upwelling sediments from the Gulf of California. In: Summerhayes, C.P., Shackleton, N.J. (Eds.), North Atlantic Palaeoceanography, vol. 21. Geological Society Special Publication, pp. 447–462.

Brumsack, H.-J., 1989. Geochemistry of recent TOC-rich sediments from the Gulf of California and the Black Sea. Geol. Rundsch. 78, 851–882.

Brumsack, H.-J., 2006. The trace metal content of recent organic carbon-rich sediments: implications for cretaceous black shale formation. Palaeogeogr. Palaeoclimatol. Palaeoecol. 232, 344–361.
Brumsack, H.-J., Gieskes, J.M., 1983. Interstitial water trace-element chemistry of laminated sediments of the Gulf of California (Mexico). Mar. Chem. 14, 89–106.
Burgener, L., Hyland, E., Reich, B.J., Scotese, C., 2023. Cretaceous climates: Mapping paleo-Köppen climatic zones using a Bayesian statistical analysis of lithologic, paleontologic, and geochemical proxies. Palaeogeogr. Palaeoclimatol. Palaeoecol. 613, 111373.
Calvert, S.E., Pedersen, T.F., 1993. Geochemistry of recent oxic and anoxic marine sediments: implications for the geological record. Mar. Geol. 113, 67–88.
Calvert, S.E., Pedersen, T.F., 1996. Sedimentary geochemistory of manganese: implications for the environment of formation of manganiferous black shales. Econ. Geol. 91, 36–47.
Calvert, S.E., Pedersen, T.F., 2007. Elemental proxies for palaeoclimatic and palaeoceanographic variability in marine sediments: Interpretation and application. In: Hillaire-Marcel, C., de Vernal, A. (Eds.), Proxies in Late Cenozoic Paleoceanography. Elsevier, New York, NY, pp. 567–644.
Castro, J.M., de Gea, G.A., Quijano, M.L., Aguado, R., Froehner, S., Naafs, B.D.A., Pancost, R.D., 2019. Complex and protracted environmental and ecological perturbations during OAE 1a- evidence from an expanded pelagic section from South Spain (Western Tethys). Glob. Planet. Chang. 183, 103030.
Caus, E., Bernaus, J.M., Calonge, E., Martín-Chivelet, J., 2009. Mid-Cenomanian separation of Atlantic and Tethyan domains in Iberia by a land-bridge: the origin of larger foraminifera provinces? Palaeogeogr. Palaeoclimatol. Palaeoecol. 283, 172–181.
Channel, J.E.T., D'Argenio, B., Horvath, F., 1979. The African Promontory, in Mesozoic Mediterranean Paleogeography. Earth Sci. Rev. 15, 213–272.
Clarke, L.J., Jenkyns, H.C., 1999. New oxygen isotope evidence for long-term cretaceous climatic change in the Southern Hemisphere. Geology 27, 699–702.
Coccioni, R., 2001. The "Pialli Level" from the Latest Albian of the Umbria-Marche Apennines. Italy. Federazione Italiana di Scienze della Terra, Geoitalia, pp. 192–193.
Coccioni, R., Galeotti, S., 2003. The mid-Cenomanian event: Prelude to OAE 2. Palaeogeogr. Palaeoclimatol. Palaeoecol. 190, 427–440.
Coccioni, R., Nesci, O., Tramontana, M., Wezel, C.F., Moretti, E., 1987. Descrizione di un livelloguida "Radiolaritico-Bituminoso-Ittiolitico" alla base delle Marne a Fucoidi nell'Appennino Umbro-Marchigiano. Boll. Soc. Geol. Ital. 106, 183–192.
Coccioni, R., Franchi, R., Nesci, O., Wezel, F.C., Battistini, F., Pallecchi, P., 1989. Stratigraphy and mineralogy of the Selli Level (Early Aptian) at the base of the Marne a Fucoidi in the Umbro-Marchean Apennines, Italy. In: Wiedmann, J. (Ed.), Cretaceous of the Western Tethys. Proceedings 3rd International Cretaceous Symposium, Tübingen 1987. E. Schweizerbartsche Verlagsbuchhandlung, Stuttgart, Germany, pp. 563–584.
Coccioni, R., Galeotti, S., Ragni, D., 1992. Litho- and biostratigraphy of the Scaglia Bianca Formation (late Albian-late Cenomanian) in the Umbria-Marche Apennines (Italy). In: Paper Presented at the 6th Annual Meeting of IGCP 262 (Tethyan Cretaceous Correlation) "Cretaceous Facies in Orogenic Belts", Athens, 22–26 May, 1992, p. 4.
Corbin, J.C., Person, A., Iatzoura, A., Ferr'e, B., Renard, M., 2000. Manganese in pelagic carbonates: indication of major Tectonic events during the geodynamic evolution of a passive continental margin (the Jurassic European Margin of the Tethys–Ligurian Sea). Palaeogeogr. Palaeoclimatol. Palaeoecol. 156, 123–138.
Cox, R., Lowe, D.R., Cullers, R.L., 1995. The influence of sediment recycling and basement composition on evolution of mudrock chemistry in the southwestern United States. Geochim. Cosmochim. Acta 59, 2919–2940.
Cresta, S., Monechi, S., Parisi, G., 1989. Stratigrafia del Mesozoico e Cenozoico nell'area umbro-marchigiana. Itinerari geologici sull'Appennino umbromarchigiano (Italia). Mem. Descritt. della Carta Geol. d'Italia 39, 1–182.
Cruse, A.M., Lyons, T.W., 2004. Trace metal records of regional paleoenvironmental variability in Pennsylvanian (Upper Carboniferous) black shales. Chem. Geol. 206, 319–345.
Cui, Q., Zhang, J., Hu, Y., et al., 2025. Transient modeling for ocean redox conditions during the mid-cretaceous Oceanic Anoxic Event 2. Glob. Planet. Chang. 253, 104976.
Dehairs, F., Chesselet, R., Jedwab, K., 1980. Discrete suspended particles of barite and the barium cycle in the open ocean. Earth Planet. Sci. Lett. 49, 528–550.
Dercourt, J., Gaetani, M., Vrielinck, B., Barrier, E., Biju-Duval, B., Brunet, M.F., Cadet, J. P., Crasquin, S., Sandulescu, M., 2000. Atlas of Peri-Tethys, Palaeogeographical Maps. Commission de la Carte Geologique du Monde (CCGN/CGMW), Paris, France.
Dymond, J., Suess, E., Lyle, M., 1992. Barium in deep-sea sediment: a proxy for paleoproductivity. Paleoceanography 7, 163–181.
Elderfield, H., 1976. Manganese fluxes to the oceans. Mar. Chem. 4, 103–132.
Erba, E., 1988. Aptian-Albian calcareous nannofossil biostratigraphy of the Scisti a Fucoidi cored at Piobbico (Central Italy). Riv. Ital. Paleontol. Stratigr. 94, 249–284.
Erba, E., 1992. Calcareous nannofossil distribution in pelagic rhythmic sediments (Aptian-Albian Piobbico core, Central Italy). Riv. Ital. Paleontol. Stratigr. 97, 455–484.
Erba, E., 2004. Calcareous nannofossils and Mesozoic oceanic anoxic events. Mar. Micropaleontol. 52, 85–106.
Erba, E., Coccioni, R., Premoli Silva, I., 1989. The "Scisti a Fucoidi" in the Umbria-Marche area: the Apecchiese road sections. Mem. Descritt. della Carta Geol. Italiana 39, 146–164.
Erba, E., Duncan, R.A., Bottini, C., Tiraboschi, D., Weissert, H., Jenkyns, H.C., Malinverno, A., 2015. Environmental consequences of Ontong Java Plateau and Kerguelen Plateau volcanism. In: The origin, evolution, and environmental impact of oceanic large igneous provinces, Geological Society of America Special Paper, vol. 511, pp. 271–303.
Erba, E., Miniati, F., Bottini, C., 2026. Revised calcareous nannofossil biozonation of the cretaceous at low and middle latitudes. Palaeogeogr. Palaeoclimatol. Palaeoecol., 113407 https://doi.org/10.1016/j.palaeo.2025.113407.
Ferrier, K.L., Mitrovica, J.X., Perron, J.T., 2016. Climatic control of chemical weathering in watersheds. Geology 44, 855–858.
Föllmi, K.B., 2012. Early cretaceous life, climate and anoxia. Cretac. Res. 35, 230–257.
Friedrich, O., Norris, R.D., Erbacher, J., 2012. Evolution of middle to late cretaceous oceans – a 55 my record of Earth's temperature and carbon cycle. Geology 40, 107–110.
Galeotti, S., Sprovieni, M., Coccioni, R., Bellanca, A., Neri, R., 2003. Orbitally modulated black shale deposition in the upper Albian Amadeus Segment (Central Italy): a multi-proxy reconstruction. Palaeogeogr. Palaeoclimatol. Palaeoecol. 190, 441–458.
Gambacorta, G., Jenkyns, H.C., Russo, F., Tsikos, H., Wilson, P.A., Faucher, G., Erba, E., 2015. Carbon-and oxygen-isotope records of mid-cretaceous Tethyan pelagic sequences from the Umbria–Marche and Belluno Basins. Italy. Newsl. Stratigr. 48 (3), 299–323.
Gambacorta, G., Bersezio, R., Weissert, H., Erba, E., 2016. Onset and demise of cretaceous oceanic anoxic events: the coupling of surface and bottom oceanic processes in two pelagic basins of the western Tethys. Paleoceanography 31 (6), 732–757.
Gambacorta, G., Bottini, C., Brumsack, H.-J., Schnetger, B., Erba, E., 2020. Major and trace element characterization of Oceanic Anoxic Event 1d (OAE 1d): Insight from the Umbria-Marche Basin, Central Italy. Chem. Geol. 557, 119834.
Gambacorta, G., Nesi, J., Erba, E., Jenkyns, H.C., 2026. High-resolution chemostratigraphy of the Bonarelli Level (OAE 2) in the Umbria–Marche Basin (Central Italy). J. Geol. Soc. Lond. https://doi.org/10.1144/jgs2025-208.
Ganeshram, R.S., Calvert, S.E., Pedersen, T.F., Cowie, G.L., 1999. Factors controlling the burial of organic carbon in laminated and bioturbated sediments off NW Mexico: implications for hydrocarbon preservation. Geochim. Cosmochim. Acta 63, 1723–1734.
Gäng, F., Böning, P., Brüchert, V., Lahajnar, N., Pahnke, K., 2023. Critical assessment of U, Ba and Ni as redox and productivity proxies in organic-rich sediments underneath dynamic, highly productive waters. Geochim. Cosmochim. Acta 348, 206–220.
Garcia, D., Fonteilles, M., Moutte, J., 1994. Sedimentary fractionations between Al, Ti, and Zr and the genesis of strongly peraluminous granites. J. Geol. 102, 411–422.
Gingele, F.X., Zabel, M., Kasten, S., Bonn, W.J., Nürnberg, C.C., 1999. Biogenic barium as a proxy for paleoproductivity: Methods and limitations of application. In: Fischer, G., Wefer, G. (Eds.), Use of Proxies in Paleoceanography. Springer, Berlin, Heidelberg, pp. 345–364.
Giorgioni, M., Weissert, H., Bernasconi, S.M., Hochuli, P.A., Coccioni, R., Keller, C.E., 2012. Orbital control on carbon cycle and oceanography in the mid-cretaceous greenhouse. Paleoceanography 27 (1), PA1204. https://doi.org/10.1029/2011PA002163.
Giorgioni, M., Weissert, H., Bernasconi, S.M., Hochuli, P.A., Keller, C.E., Coccioni, R., Petrizzo, M.R., Lukeneder, P.A., Garcia, T.I., 2015. Paleoceanographic changes during the Albian–Cenomanian in the Tethys and North Atlantic and the onset of the Cretaceous chalk. Glob. Planet. Chang. 126, 46–61.
Giorgioni, M., Tiraboschi, D., Erba, E., Hamann, Y., Weissert, H., 2017. Sedimentary patterns and palaeoceanography of the Albian Marne a Fucoidi Formation (Central Italy) revealed by high-resolution geochemical and nannofossil data. Sedimentology 64 (1), 111–126.
Giraldo-Gómez, V.M., Petrizzo, M.R., Gambacorta, G., Bottini, C., Gilardoni, S.E., Erba, E., 2023. Benthic foraminifera across the Albian–Cenomanian transition and their paleoceanographic significance during OAE1d in the western Tethys (Umbria–Marche Basin, Italy). Palaeogeogr. Palaeoclimatol. Palaeoecol. 631, 111820.
Gradstein, F.M., Ogg, J.G., Schmitz, M.D., Ogg, G.M., 2020. Geologic Time Scale 2020. Elsevier, Oxford, p. 1300.
Graziano, R., Raspini, A., 2015. Long- and short-term hydroclimatic variabilities in the Aptian Tethys: Clues from the orbital chronostratigraphy of evaporite-rich beds in the Apennine carbonate platform (Mt. Faito, southern Italy). Palaeogeogr. Palaeoclimatol. Palaeoecol. 418, 319–343.
Grippo, A., Fischer, A.G., Hinnov, L.A., Herbert, T.D., Premoli Silva, I., 2004. Cyclostratigraphy and chronology of the Albian stage (Piobbico Italy). In: D'Argenio, B., Fischer, A.G., Premoli Silva, I., Weissert, H., Ferreri, V. (Eds.), Cyclostratigraphy: Approaches and Case Histories, vol. 81. Special Publication SEPM (Society for Sedimentary Geology), pp. 57–81.
Guieu, C., Loye-Pilot, M.-D., Ridame, C., Thomas, C., 2002. Chemical characterization of the Saharan dust end-member: Some biogeochemical implications for the western Mediterranean Sea. J. Geophys. Res. 107. https://doi.org/10.1029/2001JD000582.
Guinoiseau, D., Singh, S.P., Galer, S.J.G., Abouchami, W., Bhattacharayya, R., Kandler, K., Bristow, C., Andreae, M.O., 2022. Characterization of Saharan and Sahelian dust sources based on geochemical and radiogenic isotope signatures. Quat. Sci. Rev. 293, 107729.
Guo, H., Chen, X., Yao, H., Zhang, Y., Mills, B.J.W., Han, K., Wu, S., Yang, Y., Wang, Z., Kemp, D.B., 2024. Quantifying the pattern of organic carbon burial through cretaceous Oceanic Anoxic Event 2. Earth Sci. Rev. 257, 104903.
Handy, M.R., Schmid, S.M., Bousquet, R., Kissling, E., Bernoulli, D., 2010. Reconciling platetectonic reconstructions of Alpine Tethys with the geological–geophysical record of spreading and subduction in the Alps. Earth Sci. Rev. 102, 121–158.
Hayashi, K., Fujisawa, H., Holland, H., Ohmoto, H., 1997. Geochemistry of ~1.9 Ga sedimentary rocks from northeastern Labrador, Canada. Geochim. Cosmochim. Acta 61, 4115–4137.

Heimhofer, U., Adatte, T., Hochuli, P.A., Burla, S., Weissert, H., 2008. Coastal sediments from the Algarve: low-latitude climate archive for the Aptian-Albian. In. J. Earth Sci. (Geol. Rundschau) 97, 785–797.
Heinrichs, H., Schulz-Dobrick, B., Wedepohl, K.H., 1980. Terrestrial geochemistry of Cd, Bi, Tl, Pb, Zn and Rb. Geochim. Cosmochim. Acta 44, 1519–1533.
Herbert, T.C., Fischer, A.G., 1986. Milankovitch climatic origin of mid-cretaceous black shale rhythms in Central Italy. Nature 321, 739–743.
Herbert, T.D., Stallard, R.F., Fisher, A.G., 1986. Anoxic events, productivity rhythms, and the orbital signature in a mid-cretaceous deep-sea sequence from Central Italy. Paleoceanography 1 (4), 495–506.
Herrle, J.O., 2002. Paleoceanographic and Paleoclimatic Implications on Mid-Cretaceous Black Shale Formation in the Vocontian Basin and the Atlantic: Evidence from Calcareous Nannofossil and Stable Isotopes: Tübinger Mikropaläontologische Mitteilungen, vol. 27, p. 114.
Herrle, J.O., Mutterlose, J., 2003. Calcareous nannofossils from the Aptian–Lower Albian southeast France: paleoecological and biostratigraphic implication. Cretac. Res. 24, 1–22.
Herrle, J.O., Pross, J., Friedrich, O., Kössler, P., Hemleben, C., 2003. Forcing mechanisms for Mid-cretaceous black shale formation: evidence from the upper Aptian and lower Albian of the Vocontian Basin (SE France). Palaeogeogr. Palaeoclimatol. 190, 399–426.
Herrle, J.O., Kössler, P., Friedrich, O., Erlenkeuser, H., Hemleben, C., 2004. High-resolution carbon isotope records of the Aptian to lower Albian from SE France and the Mazagan Plateau (DSDP Site 545): a stratigraphic tool for paleoceanographic and paleobiologic reconstruction. Earth Planet. Sci. Lett. 218, 149–161.
Hetzel, A., Brumsack, H.-J., Schnetger, B., Böttcher, M.E., 2006. Inorganic geochemical characterization of lithologic units recovered during ODP Leg 207 (Demerara rise). Proc. Ocean Drill. Prog. Sci. Res. 207, 1–37.
Hetzel, A., Böttcher, M.E., Wortmann, U.G., Brumsack, H.-J., 2009. Paleo-redox conditions during OAE 2 reflected in Demerara rise sediment geochemistry (ODP Leg 207). Palaeogeogr. Palaeoclimatol. Palaeoecol. 273, 302–328.
Hochuli, P.A., Menegatti, A.P., Weissert, H., Riva, A., Erba, E., Premoli Silva, I., 1999. Episodes of high productivity and cooling in the early Aptian Alpine Tethys. Geology 27, 657–660.
Holbourn, A., Kuhnt, W., Söding, E., 2001. Atlantic paleobathymetry, paleoproductivity and paleocirculation in the late Albian: the benthic foraminiferal record. Palaeogeogr. Palaeoclimatol. Palaeoecol. 170, 171–196.
Hu, X., Cheng, W., Ji, J., 2009. Origin of cretaceous Oceanic Red Beds from the Vispi Quarry Section, Central Italy: Visible reflectance and inorganic geochemistry. In: Hu, X., Wang, C., Scott, R.W., Wagreich, M., Jansa, L. (Eds.), Cretaceous Oceanic Red Beds: Stratigraphy, Composition, Origins, and Paleoceanographic and Paleoclimatic Significance, 91. Society for Sedimentary Geology, Houston, US, pp. 183–199.
Isaacs, C.M., 1982. Influence of rock composition on kinetics of silica phase changes in the Monterey Formation, Santa Barbara area, California. Geology 10, 304–308.
Jacquet, S.H.M., Henjes, J., Dehairs, F., Worobiec, A., Savoye, N., Cardinal, D., 2007. Particulate Ba-barite and acantharians in the Southern Ocean during the European Iron Fertilization Experiment (EIFEX). J. Geophys. Res. 112, G04006. https://doi.org/10.1029/2006JG000394.
Jarvis, I., Gale, A.S., Jenkyns, H.C., Pearce, M.A., 2006. Secular variation in Late Cretaceous carbon isotopes: a new $\delta^{13}C$ carbonate reference curve for the Cenomanian–Campanian (99.6–70.6 Ma). Geol. Mag. 143, 561–608.
Jarvis, I., Lignum, J.S., Gröcke, D.R., Jenkyns, H.C., Pearce, M.A., 2011. Black shale deposition, atmospheric CO_2 drawdown, and cooling during the Cenomanian–Turonian Oceanic Anoxic Event. Paleoceanography 26, PA3201. https://doi.org/10.1029/2010PA002081.
Jenkyns, H.C., 2010. Geochemistry of oceanic anoxic events. Geochem. Geophys. Geosyst. 11, Q03004. https://doi.org/10.1029/2009GC002788.
Jenkyns, H.C., Dickson, A.J., Ruhl, M., van den Boorn, S.H.J.M., 2017. Basalt–seawater interaction, the Plenus Cold Event, enhanced weathering and geochemical change: deconstructing Oceanic Anoxic Event 2 (Cenomanian–Turonian, late cretaceous). Sedimentology 64, 16–43.
Kastner, M., Keene, J.B., Gieskes, J.M., 1977. Diagenesis of siliceous oozes–I. Chemical controls on the rate of opal-a to opal-CT transformation – an experimental study. Geochim. Cosmochim. Acta 41, 1041–1059.
Kemper, E., 1987. Das Klima der Kreide-Zeit. Geol. Jahrbuch A 96, 5–185 (in German).
Klinkhammer, G.P., Bender, M.L., 1980. The distribution of manganese in the Pacific Ocean. Earth Planet. Sci. Lett. 46, 361–384.
Klinkhammer, G.P., McManus, J., 2001. Dissolved manganese in the Columbia River estuary: production in the water column. Geochim. Cosmochim. Acta 65, 2835–2841.
Klinkhammer, G.P., Chin, C.S., Wilson, C., Rudnicki, M.D., German, C.R., 1997. Distributions of dissolved manganese and fluorescent dissolved organic matter in the Columbia River estuary and plume as determined by in situ measurement. Mar. Chem. 56, 1–14.
Klinkhammer, G.P., Mix, A.C., Haley, B.A., 2009. Increased dissolved terrestrial input to the coastal ocean during the last deglaciation. Geochem. Geophys. Geosyst. 10, Q03009. https://doi.org/10.1029/2008GC002219.
Lanci, L., Muttoni, G., Erba, E., 2010. Astronomical tuning of the Cenomanian Scaglia Bianca Formation at Furlo, Italy. Earth Planet. Sci. Lett. 292, 231–237.
Leckie, R.M., Bralower, T.J., Cashman, R., 2002. Oceanic anoxic events and plankton evolution: Biotic response to tectonic forcing during the Mid-cretaceous. Paleoceanography 17(3), 1041, 13–29.
Li, X., Wei, Z., Švábenická, L., Wang, J., Wei, S., Zhou, Y., Fan, X., Jiebu, G., Zhaxi, P., 2026. Elevated δ13C values across the Albian-Cenomanian boundary (OAE 1d) in eastern Neo-Tethys: insights into a potential super nutrient water mass. Glob. Planet. Chang. 257, 105245.
Liang, Y., Li, Y.-X., Lu, H., Wang, H., Wang, C., Quan, C., Liu, W., Zhou, M.-F., Liu, Z., 2026. Oceanic deoxygenation linked to enhanced water column stratification in the eastern Tethys during cretaceous Oceanic Anoxic Event 2. Glob. Planet. Chang. 258, 105270.
Liguori, B.T.P., De Almeida, M.G., De Rezende, C.E., 2016. Barium and its importance as an indicator of (paleo)productivity. An. Acad. Bras. Cienc. 88 (4), 2093–2103.
Maher, K., 2011. The role of fluid residence time and topographic scales in determining chemical fluxes from landscapes. Earth Planet. Sci. Lett. 312, 48–58.
Matsumoto, H., Kuroda, J., Coccioni, R., Frontalini, F., Sakai, S., Ogawa, N.O., Ohkouci, N., 2020. Marine Os isotopic evidence for multiple volcanic episodes during C retaceous Oceanic Anoxic Event 1b. Sci. Rep. 2020, 12601. https://doi.org/10.1038/s41598-020-69505-x.
McAnena, A., Flögel, S., Hofmann, P., Herrle, J.O., Griesand, A., Pross, J., Talbot, H.M., Rethemeyer, J., Wallmann, K., Wagner, T., 2013. Atlantic cooling associated with a marine biotic crisis during the mid-cretaceous period. Nat. Geosci. 6, 558–651.
McManus, J., Berelson, W.M., Klinkhammer, G.P., Johnson, K.S., Coale, K.H., Anderson, R.F., Kumar, N., Burdige, D.J., Hammond, D.E., Brumsack, H.-J., McCorkle, D.C., Rushdi, A., 1998. Geochemistry of barium in marine sediments: implications for its use as a paleoproxy. Geochim. Cosmochim. Acta 62, 3453–3473.
Meinhardt, A.-K., Pahnke, K., Böning, P., Schnetger, B., Brumsack, H.-J., 2016. Climate change and response in bottom water circulation and sediment provenance in the Central Arctic Ocean since the last Glacial. Chem. Geol. 427, 98–108. https://doi.org/10.1016/j.chemgeo.2016.02.019.
Mendez, J., Guieu, C., Adkins, J., 2010. Atmospheric input of manganese and iron to the ocean: Seawater dissolution experiments with Saharan and north American dusts. Mar. Chem. 120 (1–4), 34–43.
Menegatti, A.P., Weissert, H., Brown, R.S., Tyson, R.V., Farrimond, P., Strasser, A., Caron, M., 1998. High-resolution $\delta^{13}C$ stratigraphy through the early Aptian Livello Selli of the Alpine Tethys. Paleoceanography 13, 530–545.
Millán, M.I., Weissert, H.J., López-Horgue, M.A., 2014. Expression of the late Aptian cold snaps and the OAE1b in a highly subsiding carbonate platform (Aralar, northern Spain). Palaeogeogr. Palaeoclimatol. 411, 167–179.
Moreno, T., Querol, Z., Castillo, S., Alastuey, A., Cuevas, E., Herrmann, L., Mounkaila, M., Elvira, J., Gibbons, W., 2006. Geochemical variations in aeolian mineral particles from the Sahara–Sahel Dust Corridor. Chemosphere 65, 261–270.
Morford, J.L., Emerson, S., 1999. The geochemistry of redox sensitive trace metals in sediments. Geochim. Cosmochim. Acta 63, 1735–1750.
Morford, J.L., Russell, A.D., Emerson, S., 2001. Trace metal evidence for changes in the redox environment associated with the transition from terrigenous clay to diatomaceous sediments, Saanich Inlet, BC. Mar. Geol. 174, 355–369.
Muhs, D.R., Budahn, J., Skipp, G., Prospero, J.M., Patterson, D., Bettis III, E.A., 2010. Geochemical and mineralogical evidence for Sahara and Sahel dust additions to Quaternary soils on Lanzarote, eastern Canary Islands, Spain. Terra Nova 22, 399–410.
Mutterlose, J., Bornemann, A., Herrle, J., 2009. The Aptian–Albian cold snap: evidence for "mid" Cretaceous icehouse interludes. N. Jb. Geol. Paläont. 252, 217–225.
O'Brien, C.L., Robinson, S.A., Pancost, R.D., Damsté, J.S.S., Schouten, S., Lunt, D.J., Alsenz, H., Bornemann, A., Bottini, C., Brassell, S.C., Farnsworth, A., Forster, A., Huber, B.T., Inglis, G.N., Jenkyns, H.C., Linnert, C., Littler, K., Markwick, P., McAnena, A., Mutterlose, J., Naafs, B.D.A., Püttmann, W., Sluijs, A., van Helmond, A.G.M., Vellecoop, J., Wagner, T., Wrobel, N.E., 2017. Cretaceous sea-surface temperature evolution: Constraints from TEX86 and planktonic foraminiferal oxygen isotopes. Earth Sci. Rev. 172, 224–247.
Parisi, G., Baldanza, A., Monechi, S., 1989. Da Gubbio a Scheggia. Mem. Descritt. della Carta Geol. d'Italia 39, 50–56.
Paytan, A., Griffith, E.M., 2007. Marine barite: Recorder of variations in ocean export productivity. Deep-Sea Res. Pt. II 54, 687–705.
Pedersen, T.F., Price, N.B., 1982. The geochemistry of manganese carbonate in Panama Basin sediments. Geochim. Cosmochim. Acta 46, 59–68.
Petrizzo, M.R., Gilardoni, S.E., 2020. Planktonic foraminiferal biostratigraphy of late Albian–Cenomanian pelagic sequences from the Umbria–Marche Basin (central Italy) and the Mazagan Plateau (northeast Atlantic Ocean). Riv. Ital. Paleontol. Stratigr. 126 (3), 865–904. https://doi.org/10.13130/2039-4942/14493.
Piper, D.Z., Perkins, R.B., 2004. A modern vs. Permian black shale— the hydrography, primary productivity, and water-column chemistry of deposition. Chem. Geol. 206, 177–197.
Pratt, L.M., King, J.D., 1986. Variable marine productivity and high eolian input recorded by rhythmic black shales in mid-cretaceous pelagic deposits from Central Italy. Paleoceanography 1 (4), 507–522.
Premoli Silva, I., Erba, E., Tornaghi, M.E., 1989. Paleoenvironmental signals and changes in surface fertility in mid-cretaceous Corgrich pelagic facies of the Fucoid Marls (Central Italy). Geobios, Mém. Spéc. 11, 225–236.
Premoli Silva, I., Erba, E., Salvini, G., Verga, D., Locatelli, C., 1999. Biotic changes in cretaceous anoxic events. J. Foraminifer. Res. 29, 352–370.
Price, G.D., 1999. The evidence and implications of polar ice during the Mesozoic. Earth Sci. Rev. 48, 183–210.
Rachold, V., Brumsack, H.-J., 2001. Inorganic geochemistry of Albian sediments from the Lower Saxony Basin NW Germany: palaeoenvironmental constraints and orbital cycles. Palaeogeogr. Palaeoclimatol. Palaeoecol. 174, 121–143.
Rajendran, A., Dileepkumar, M., Bakker, J.F., 1992. Control on manganese and iron in Skagerrak sediment (northeastern North- Sea). Chem. Geol. 98, 111–129.
Robinson, S.A., Clarke, L.J., Nederbragt, A., Wood, I.G., 2008. Mid-cretaceous oceanic anoxic events in the Pacific Ocean revealed by carbon-isotope stratigraphy of the Calera Limestone, California, USA. Geol. Soc. Am. Bull. 120 (11−12), 1416–1426.

Rodríguez-López, J.P., de Boer, P.L., Meléndez, N., Soria, A.R., Pardo, G., 2006. Windblown desert sands in coeval shallow marine deposits: a key for the recognition of coastal ergs in the mid-cretaceous Iberian Basin, Spain. Terra Nova 18, 314–320.
Rodríguez-López, J.P., Liesa, C.L., Pardo, G., Meléndez, N., Soria, A.R., Skilling, I., 2016. Glacial dropstones in the western Tethys during the late Aptian–early Albian cold snap: Palaeoclimate and palaeogeographic implications for the mid-cretaceous. Palaeogeogr. Palaeoclimatol. Palaeoecol. 452, 11–27.
Sabatino, N., Coccioni, R., Manta, D.S., Baudin, F., Vallefuoco, M., Traina, A., Sprovieri, M., 2015. High-resolution chemostratigraphy of the late Aptian–early Albian oceanic anoxic event (OAE 1b) from the Poggio le Guaine section (Umbria–Marche Basin, Central Italy). Palaeogeogr. Palaeoclimatol. Palaeoecol. 426, 319–333.
Sabatino, N., Ferraro, S., Coccioni, R., Bonsignore, M., Del Core, M., Tancredi, V., Sprovieri, M., 2018. Mercury anomalies in upper Aptian-lower Albian sediments from the Tethys realm. Palaeogeogr. Palaeoclimatol. Palaeoecol. 495, 163–170.
Sageman, B.B., Lyons, T.W., 2005. Geochemistry of fine-grained sediments and sedimentary rocks. In: Holland, H.D., Turekian, K.K. (Eds.), Sediments, Diagenesis, and Sedimentary Rocks. Treatise on Geochemistry, 7. Elsevier, Amsterdam, pp. 115–158.
Schlanger, S.O., Jenkyns, H.C., 1976. Cretaceous oceanic anoxic events: causes and consequences. Geol. Mijnb. 55, 179–184.
Schmitz, B., Charisi, S.D., Thompson, E.I., Speijer, R.P., 1997. Barium, SiO_2 (excess), and P_2O_5 as proxies of biological productivity in the Middle East during the Palaeocene and the latest Palaeocene benthic extinction event. Terra Nova 9, 95–99.
Schneider, R.R., Price, B., Müller, P.J., Kroon, D., Alexander, I., 1997. Monsoon related variations in Zaire (Congo) sediment load and influence of fluvial silicate supply to productivity in the east equatorial Atlantic during the last 200,000 years. Paleoceanography 12, 463–481.
Schnetger, B., 1992. Chemical composition of loess from a local and wordwide view. Neues Jahrbuch Mineralogische Abhandlungen, Monatshefte H. 1 29–47.
Schnetger, B., Brumsack, H.-J., Schale, H., Hinrichs, J., Dittert, L., 2000. Geochemical characteristics of deep-sea sediments from the Arabian Sea: a high-resolution study. Deep-Sea Res. II 47, 2735–2768.
Schoepfer, S.D., Shen, J., Wei, H.Y., Tyson, R.V., Ingall, E., Algeo, T.J., 2015. TOC, organic P, and biogenic Ba accumulation rates as proxies for marine primary productivity and export flux. Earth Sci. Rev. 149, 23–52.
Scholle, P.A., Arthur, M.A., 1980. Carbon isotope fluctuation in cretaceous pelagic limestones: potential stratigraphic and petroleum exploration tool. Am. Assoc. Pet. Geol. Bull. 64, 67–87.
Schwarzacher, W., 1994. Cyclostratigraphy of the Cenomanian in the Gubbio district, Italy: A field study. In: de Boer, P.L., Smith, D.G. (Eds.), Orbital Forcing and Cyclic Sequences, vol. 19. Special Publication International Association of Sedimentologists, Gent, Belgium, pp. 99–107.
Scotese, C.R., Song, H., Mills, B.J.W., van der Meer, D.G., 2021. Phanerozoic paleotemperatures: the earth's changing climate during the last 540 million years. Earth-Sci. Rev. 215, 103503.
Scotese, C.R., Vérard, C., Burgener, L., Elling, R.P., Kocsis, A.T., 2025. The cretaceous world: Plate tectonics, palaeogeography and palaeoclimate. In: Hart, M.B., Batenburg, S.J., Huber, B.T., Price, G.D., Thibault, N., Wagreich, M., Walaszczyk, I. (Eds.), Cretaceous Project 200 Volume 1: the Cretaceous World, Vol. 544. Geological Society, London, Special Publications, London, UK, pp. 31–202.
Sequero, C., Froehner, S., Castro, J.M., De Gea, G.A., Quijano, M.L., Naafs, B.D.A., Pancost, R.D., 2026. Immediate and delayed biotic and environmental responses to the carbon cycle perturbation at the onset of OAE 1a – insights from a new high-resolution record from the Western Tethys. Glob. Planet. Chang. 256, 105170.
Sherman, D.D., 1952. Chemical weathering and landforms. Geol. Soc. Am. Bull. 63, 1281–1302.
Shiller, A.M., 1997. Manganese in surface waters of the Atlantic Ocean. Geophys. Res. Lett. 24, 1495–1498.
Skelton, P.W., Spicer, R.A., Kelley, S.P., Gilmour, I., 2003. The Cretaceous World. Cambridge Univ. Press, Cambridge, U.K.
Stallard, R.F., 1985. River chemistry, geology, geomorphology, and soils in the Amazon and Orinoco basins. In: Drever, J.I. (Ed.), The Chemistry of Weathering. D. Reidel Publishing Company, Dordrecht, pp. 293–316.
Tejada, M.L.G., Suzuki, K., Kuroda, J., Coccioni, R., Mahoney, J.J., Ohkouchi, N., Sakamoto, T., Tatsumi, Y., 2009. Ontong Java Plateau eruption as a trigger for the early Aptian oceanic anoxic event. Geology 37, 855–858.
Thyberg, B.I., Jordt, H., Bjørlykke, K., Faleide, J.I., 2000. Relationships between sequence stratigraphy, mineralogy and geochemistry in Cenozoic sediments of the northern North Sea. In: Nøttvedt, A. (Ed.), Dynamics of the Norwegian Margin, vol. 167. Geological Society, London, Special Publications, London, pp. 245–272.
Tiraboschi, D., Erba, E., Jenkyns, H.C., 2009. Origin of rhythmic Albian black shales (Piobbico core, Central Italy): Calcareous nannofossil quantitative and statistical analyses and paleoceanographic reconstructions. Paleoceanography 24, PA2222. https://doi.org/10.1029/2008PA001670.
Tornaghi, M.E., Premoli Silva, I., Ripepe, M., 1989. Lithostratigraphy and planktonic foraminiferal biostratigraphy of the Aptian-Albian "Scisti a Fucoidi" in the Piobbico Core, Marche, Italy: background for cyclostratigraphy. Riv. Ital. Paleontol. Stratigr. 95, 223–264.
Torres, M.E., Brumsack, H.J., Bohrmann, G., Emeis, K.C., 1996. Barite fronts in continental margin sediments: a new look at barium remobilization in the zone of sulfate reduction and formation of heavy barites in diagenetic fronts. Chem. Geol. 127, 125–139.
Tribovillard, N., Algeo, T.J., Lyons, T., Riboulleau, A., 2006. Trace metals as paleoredox and paleoproductivity proxies: an update. Chem. Geol. 232, 12–32. https://doi.org/10.1016/j.chemgeo.2006.02.012.
Turgeon, S., Brumsack, H.-J., 2006. Anoxic vs dysoxic events reflected in sediment geochemistry during the Cenomanian–Turonian Boundary Event (Cretaceous) in the Umbria–Marche Basin of central Italy. Chem. Geol. 234, 321–339.
van Hulten, M., Middag, R., Dutay, J.-C., de Baar, H., Roy-Barman, M., Gehlen, M., Tagliabue, A., Sterl, A., 2017. Manganese in the West Atlantic Ocean in the context of the first global ocean circulation model of manganese. Biogeosciences 14, 1123–1152.
Wang, X., Lang, L., Hua, T., Zhang, C., Li, H., 2017. The effects of sorting by aeolian processes on the geochemical characteristics of surface materials: a wind tunnel experiment. Front. Earth Sci. 12 (1), 86–94.
Wedepohl, K.H., 1971. Environmental influences on the chemical composition of shales and clays. In: Ahrens, L.H., Press, F., Runcorn, S.K., Urey, H.C. (Eds.), Physics and Chemistry of the Earth, Vol. vol. 8. Pergamon, Oxford, UK, pp. 305–333.
Wedepohl, K.H., 1991. The composition of the upper earth's crust and the natural cycles of selected metals. Metals in natural raw materials. Natural resources. In: Merian, E. (Ed.), Metals and their Compounds in the Environment. VCH, Weinheim, pp. 3–17.
Wehausen, R., Tian, J., Brumsack, H.-J., Cheng, X., Wang, P., 2003. Geochemistry of Pliocene sediments from ODP Site 1143 (southern South China Sea). In: Prell, W.L., Wang, P., Blum, P., Rea, D.K., Clemens, S.C. (Eds.), Proc. ODP, Sci. Results, 184, 1–25 [Online].
Weissert, H., 1989. C-isotope stratigraphy, a monitor of paleoenvironmental change: a case study from the early cretaceous. Surv. Geophys. 10, 1–61.
Weissert, H., Lini, A., 1991. Ice age interludes during the time of cretaceous greenhouse climate. In: Mtiller, D.W., McKenzie, I.A., Weissert, H. (Eds.), Controversies in Modem Geology. Academic Press, London, pp. 173–191.
White, A.F., Blum, A.E., 1995. Effects of climate on chemical weathering in watersheds. Geochim. Cosmochim. Acta 59, 1729–1747.
Williams, L.A., Parks, G.A., Crerar, D.A., 1985. Silica diagenesis, I. Solubility controls. J. Sediment. Petrol. 55, 301–311.
Wilson, P.A., Norris, R.D., 2001. Warm tropical ocean surface and global anoxia during the mid-cretaceous period. Nature 412, 425–429.
Zhang, Y., Mahowald, N., Scanza, R., Journet, E., Desboeufs, K., Albani, S., Kok, J., Zhuang, G., Chen, Y., Cohen, D.D., Paytan, A., Patey, M.D., Achterberg, E.P., Engelbrecht, J.P., Fomba, K.W., 2015. Modeling the global emission, transport and deposition of trace elements associated with mineral dust. Biogeosciences 12 (19), 5771–5792.
Zhang, Y., Yao, H., Zhang, Y., Bown, P.R., Grasby, S.E., Yin, R., Han, K., Guo, H., Wang C., Chen, X., 2026. Quantifying volcanism during Oceanic Anoxic Event 2 constrained by sedimentary mercury. Glob. Planet. Chang. 257, 105207.
Zimmerli, G.N., Wohlwend, S., Deplazes, G., Becker, J., Wetzel, A., Francescangeli, F., Foubert, A., 2024. Facies variability and depositional cyclicity in central Northern Switzerland: insights from new Opalinus Clay drill cores. Swiss J. Geosci. 117, 18. https://doi.org/10.1186/s00015-024-00463-6.